de Haas–van Alphen Effect in Pyrolytic and Single-Crystal Graphite*

S. J. WILLIAMSON† AND S. FONER
National Magnet Laboratory,†‡ Massachusetts Institute of Technology, Cambridge, Massachusetts

AND

M. S. DRESSELHAUS§
Lincoln Laboratory,‖ Massachusetts Institute of Technology, Lexington, Massachusetts

(Received 17 June 1965)

The de Haas–van Alphen (DHVA) oscillations have been observed in the differential susceptibility of well-annealed pyrolytic graphite (PG) with the low-frequency field-modulation technique. The results for PG are compared with similar studies of natural single crystal (SCG) by Soule *et al.*, and by the present authors. Majority-electron and majority-hole DHVA periods in PG are respectively equal to the periods in SCG for $0°\lesssim\theta\lesssim 50°$, where θ is the angle between the applied field and the c axis of the sample. Observation of a long-period, minority-carrier DHVA oscillation in PG and SCG confirms Soule's discovery of such an oscillation in SCG and provides a sensitive test for the Slonczewski-Weiss band model. The minority-carrier oscillation in PG is qualitatively but not quantitatively similar to the one in SCG. This oscillation is attributed to magnetic energy levels passing through the Fermi level near the Brillouin-zone corner at $k_z=\pi/c_0$, where for $\theta=0°$ there is *no* extremal area of the Fermi surface at zero field, when spin-orbit interactions are neglected. This interpretation is supported by the calculation of an oscillatory free energy and by the excellent agreement for PG between the predicted values and experimental results for the period, effective mass, period anisotropy, and phase. The phase is not the value which would be predicted from a free-electron model for either a maximal or a minimal cross-sectional area. The existence of minority-carrier oscillations in PG indicates that the hole and electron Fermi surfaces are closed and that the electron surface intersects the hexagonal face of the Brillouin zone. The band parameters of the Slonczewski-Weiss model for PG were evaluated from the DHVA data and the preliminary magnetoreflection measurements of Dresselhaus and Mavroides. A similar analysis for SCG was carried out successfully for the majority-carrier pockets, but did not provide a consistent picture for the minority-carrier surface. The effects of spin-orbit interaction on the Fermi surface are discussed. Neutron and x-ray diffraction studies show that the c axes of the individual crystallites in a PG sample are aligned to no better than $\sim 1°$. The effects of this misalignment as well as of the finite crystallite size on the DHVA oscillations are considered.

I. INTRODUCTION

PYROLYTIC graphite (PG) is a polycrystalline material that exhibits substantial order and can be fabricated with large dimensions. Numerous investigations of its electrical and thermal conductivity have indicated that the temperature dependences of these transport properties qualitatively approach the behavior of these respective properties in natural single-crystal graphite (SCG) as the annealing temperature of the PG is increased.[1,2] This increase in similarity coincides with an increase in the size and improvement in the relative orientation of the individual crystallites. The present de Haas–van Alphen (DHVA) experiments were undertaken to make a detailed comparison of the Fermi surfaces and of the electronic band structure of PG with that of SCG.

DHVA-type oscillations due to two majority carriers were first observed in SCG by Shoenberg,[3] and have been studied more recently by several other investigators.[4–6] The most complete and detailed investigation of SCG to date has been performed in the Shubnikov–de Haas experiments of Soule, McClure, and Smith.[7] This, together with DHVA experiments on SCG by Soule,[8] in which the minority carrier oscillations were first observed, and with experiments on SCG that we have conducted will form the standard by which we will compare our PG results. The present investigation[9] in PG permitted an assessment of the applicability to SCG of the extensive band parameter evaluations by Dresselhaus and Mavroides[10] based on analysis of the magnetoreflection experiments on PG. The results show that general features of the majority carrier pockets are identical for SCG and PG whereas details near the zone corners differ appreciably.

In addition, the results of the present experiments

* A portion of this paper is based on a thesis submitted by one of the authors (S. J. Williamson) in partial fulfillment for the degree of Sc.D. in the Department of Physics at the Massachusetts Institute of Technology, May 1965.

† National Science Foundation and Danforth Foundation Predoctoral Fellow.

‡ Supported by the U. S. Air Force Office of Scientific Research.

§ Visiting Scientist, National Magnet Laboratory.

‖ Operated with support from the U. S. Air Force.

[1] C. A. Klein, W. D. Straub, and R. J. Diefendorf, Phys. Rev. **125**, 468 (1962).

[2] C. A. Klein, Rev. Mod. Phys. **34**, 56 (1962).

[3] D. Shoenberg, Phil. Trans. Roy. Soc. London **A245**, 1 (1952).

[4] T. G. Berlincourt and M. C. Steele, Phys. Rev. **98**, 956 (1955).

[5] D. E. Soule, Phys. Rev. **112**, 698, 708 (1958).

[6] W. J. Spry and P. M. Scherer, Phys. Rev. **120**, 826 (1960).

[7] D. E. Soule, J. W. McClure, and L. B. Smith, Phys. Rev. **134**, A453 (1964).

[8] D. E. Soule, IBM J. Res. Develop. **8**, 268 (1964).

[9] S. J. Williamson, S. Foner, and M. S. Dresselhaus, in *Proceedings of the Ninth International Conference on Low Temperature Physics, Columbus, Ohio, 1964*, edited by J. G. Daunt, D. V. Edwards, F. J. Milford, and M. Yagub (Plenum Press, Inc., New York, 1965); Bull. Am. Phys. Soc. **10**, 109 (1965).

[10] M. S. Dresselhaus and J. G. Mavroides, IBM J. Res. Develop. **8**, 262 (1964).

have provided a sensitive test of the Slonczewski-Weiss band model for graphite.[11] Graphite is the semimetal for which the band structure has probably been analyzed most extensively on the basis of general principles—the experimental data are used not for establishment of the dispersion relations and Fermi surface but also for the determination of its band parameters. Verification that the experimental results agree with the theoretical predictions of the band model is therefore of fundamental importance. During the course of the present experiments a long-period DHVA oscillation was observed which in some respects is similar to the minority carrier oscillation discovered in the susceptibility studies of SCG by Soule.[8] This long-period oscillation is identified with a nonstationary Fermi surface cross section at the zone boundary $k_z=\pi/c_0$. The justification for this identification is the stationary character at $k_z=\pi/c_0$ of the magnetic energy levels in the absence of spin-orbit interaction[12,13] and the extremal character of the Fermi surface cross section itself when spin-orbit interaction is included.[14] Furthermore, this interpretation gives excellent agreement between experiment and the predictions of the Slonczewski-Weiss band model for the DHVA period, anisotropy and effective mass, using band parameters which are consistent with the preliminary magnetoreflection analysis of Dresselhaus and Mavroides.[10] This agreement thus demonstrates the applicability of the Slonczewski-Weiss band model to PG. Furthermore, this interpretation shows that the electron and hole Fermi surfaces are closed, and that the electron surface intersects the hexagonal face of the Brillouin zone.

An important aspect of the present investigation is a comparison of the observed phases of the majority and minority carrier oscillations in PG with those predicted by the Slonczewski-Weiss model. The agreement is excellent, thus indicating that the effect of possible electron-electron interactions on the phases are negligible for this material. In addition, the fact that the phase of the minority carrier oscillations corresponds to neither that predicted by the Onsager-Lifshitz condition for free electrons nor that for a maximum or minimum of the cross-sectional area of the Fermi surface, and yet is given correctly by the Slonczewski-Weiss model lends added support to our interpretation.

Section II contains a brief description of the de Haas–van Alphen effect, and Sec. III, those aspects of the graphite band structure which are relevant to this effect. This is followed in Sec. IV by a description of the PG samples used in the present experiments, including x-ray and neutron-diffraction studies, and in Sec. V by a brief discussion of the experimental techniques. The interpretation of the experimental results is divided into three sections: comparisons of majority carrier oscillations in PG and SCG (Sec. VI); examination of the effects of the polycrystalline nature of PG on the DHVA oscillations (Sec. VII); and development of a Fermi surface model for the explanation of the long-period, minority-carrier oscillations with a subsequent discussion of the implications of this model (Sec. VIII). The criterion for the observation of a DHVA oscillation at a stationary point in the magnetic energy levels is established by direct calculation in an Appendix.

II. THEORETICAL ASPECTS OF THE DE HAAS–VAN ALPHEN EFFECT

The DHVA effect is used to compare the electronic band structures of PG and SCG in the present experiments because it permits a detailed investigation of the Fermi surface. For an arbitrary Fermi surface, the oscillatory component of the electronic thermodynamic potential Ω was first derived by Lifshitz and Kosevich[15] and has since been refined by various other authors.[16–19] This oscillatory-magnetic-field dependence is related to the extremal area A of the Fermi surface cross section in k space normal to the magnetic induction $\mathbf{B}=B\mathbf{z}$ by the formula

$$(\Omega)_{\rm osc}=2VkT(eB/hc)^{3/2}\left[\partial^2 A/\partial k_z^2\right]_{k_m}^{-1/2} \times\sum_{j=1}^{\infty}\frac{\exp(-2\pi^2 jkT_D/\beta^* B)}{j^{3/2}\sinh(2\pi^2 jkT/\beta^* B)} \times\cos\left[\frac{j\hbar c}{eB}A-2\pi j\gamma\mp\frac{\pi}{4}\right]\cos\left[\frac{j\pi g m^*}{2m_0}\right], \tag{1}$$

in which $k_z=k_m$ defines the location of the extremal area, β^* is the effective double Bohr magneton $\beta^*=e\hbar/m^*c$, m^* is the effective mass $m^*=\hbar^2\partial A/2\pi\partial\zeta$ where ζ is the Fermi energy, T_D is the Dingle temperature related to the width $\hbar/\tau$ of the Landau levels given by $kT_D=\hbar/\pi\tau$,[17,18] g is the spin-splitting factor,[16] and m_0 is the free-electron mass. The upper or lower signs in the phase correspond to a maximum or minimum, respectively, in the extremal cross-sectional area of the Fermi surface. The parameter γ enters the theory from

[11] J. C. Slonczewski and P. R. Weiss, Phys. Rev. **109**, 272 (1958).
[12] J. W. McClure, Phys. Rev. **119**, 606 (1960).
[13] M. Inoue, J. Phys. Soc. Japan **17**, 808 (1962).
[14] G. Dresselhaus and M. S. Dresselhaus, Phys. Rev. **140**, A401 (1965). The effects of spin-orbit splitting on the energy levels at the corner of the Brillouin zone in some of the hexagonal-close-packed metals have been considered previously by L. M. Falicov and M. H. Cohen, Phys. Rev. **130**, 92 (1963) using an OPW approximation.
[15] I. M. Lifshitz and A. M. Kosevich, Zh. Eksperim. i Teor. Fiz. **29**, 730 (1955) [English transl.: Soviet Phys.—JETP **2**, 636 (1956)].
[16] M. H. Cohen and E. I. Blount, Phil. Mag. **5**, 115 (1960).
[17] R. B. Dingle, Proc. Roy. Soc. (London) **A211**, 500, 512 (1952).
[18] S. J. Williamson, S. Foner, and R. A. Smith, Phys. Rev. **136**, A1065 (1964).
[19] Summaries of experimental and theoretical progress made in understanding the DHVA effect have been given by D. Shoenberg, in *Progress in Low Temperature Physics* (North-Holland Publishing Company, Amsterdam, 1957), Vol. II, p. 226, and may also be found in the first part of Ref. 9.

the Onsager-Lifshitz quantization condition[20,21] for coincidence of a Landau level with the Fermi level.

$$A=2\pi(n+\gamma)eB/\hbar c, \qquad (2)$$

and $\gamma=\frac{1}{2}$ for free electrons. If A is independent of B, the oscillations of Ω and hence of the magnetic susceptibility are periodic in B^{-1} with a period $P=2\pi e/\hbar cA$. Generally, the phase of a DHVA oscillation (and therefore also the parameter γ) is difficult to measure accurately unless oscillations can be observed near the low-quantum limit. However, in the low-quantum limit for majority-carrier pockets, the Fermi energy ζ (and consequently A) may be field-dependent so that the DHVA oscillations are no longer periodic in B^{-1}. The parameters of interest in the present experiments are A, m^*, T_D, and γ.

III. BAND THEORY OF GRAPHITE

The effective-mass Hamiltonian which describes the energy bands of graphite was first derived by Slonczewski and Weiss[11] and was developed further by McClure.[22] Earlier calculations by Wallace, Coulson and Taylor, Lomer, Corbato, and Johnson,[11] using for the most part tight-binding arguments, showed that current carriers in this hexagonal close-packed structure occupy only a small fraction of the hexagonal Brillouin zone (shown in Fig. 1) and that only the π bands near the vertical edges of the zone are important for the determination of the transport properties. These facts are used to derive an effective-mass Hamiltonian for the energy bands near the vertical edges, using the symmetry properties of the graphite lattice. Electron-electron correlations are neglected. The $\mathbf{k}\cdot\mathbf{p}$ perturbation method is used to derive the form of the energy bands away from the vertical edges. In the z direction, along the c axis of the sample, the matrix elements in the one-electron Hamiltonian are expanded in a Fourier

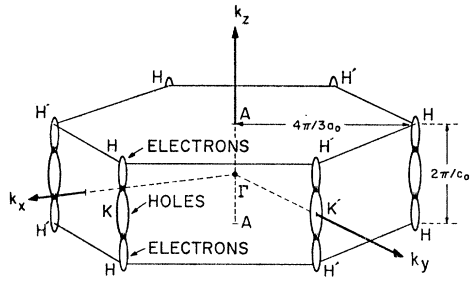

FIG. 1. Brillouin zone of graphite. The lattice parameters are $a_0=2.456$ Å and $c_0=6.712$ Å for single-crystal graphite, where c_0 is twice the distance between layer planes. Electron and hole pockets formed by the π bands are centered on the vertical zone edges HKH.

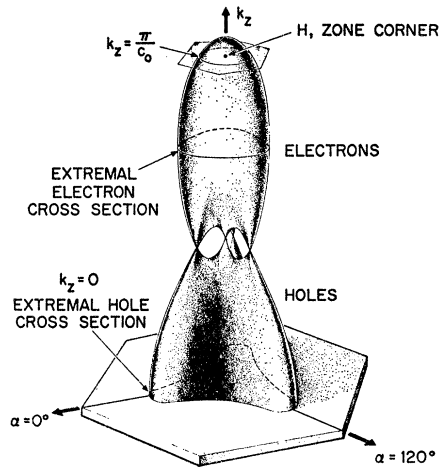

FIG. 2. Fermi surface of graphite. Electron and hole surfaces for $k_z>0$ at the vertical zone edge HKH are shown in an extended zone scheme. The trigonal warping of the surfaces, which is most pronounced at $k_z=0$, is caused by an interaction characterized by the band parameter γ_3. To emphasize this trigonal anisotropy, the scale perpendicular to the k_z axis has been expanded by a factor of 5. This figure is similar to one published by M. S. Dresselhaus and J. G. Mavroides, IBM J. Res. Develop. 8, 262 (1964).

series (in the spirit of the tight-binding approximation) which is rapidly convergent due to the large separation of layer planes. The determination of the band structure is thus reduced to finding numerical values for the matrix elements of the effective-mass Hamiltonian. A physical interpretation of these matrix elements as overlap integrals of energy and momentum can be found by using tight-binding arguments.[23]

The four π bands obtained from this theory give rise to electron and hole pockets strung in "sausage" fashion along the vertical zone edges HKH as shown in Fig. 1. The details of the Fermi surface structure near these zone edges is illustrated for an extended zone scheme in Fig. 2 for the warped ellipsoid picture developed by Nozières[24] and McClure.[22]

The hexagonal lattice of graphite has a Bernal-type stacking of the layers corresponding to a sequence $1212\cdots$.[25] The centers of the hexagons in one layer lie over corners of the hexagons in the layer beneath. There are therefore two inequivalent lattice sites in each layer, A atoms which have A' atoms directly above and below them in neighboring layers, and B atoms which have no atoms above or below in neighboring layers. The unit cell is characterized by the parameters $a_0=2.456$ Å and $c_0=6.712$ Å,[26] where c_0 is twice the spacing between layers. In describing the band structure in the reciprocal space which corresponds to this

[20] L. Onsager, Phil. Mag. 43, 1006 (1952).
[21] I. M. Lifshitz, Report to the Phys. Math. Section, Academy of Sciences, Ukr. SSR, Dec. 1951; quoted by I. M. Lifshitz and M. I. Kaganov, Usp. Fiz. Nauk 69, 419 (1959) [English transl.: Soviet Phys.— 2, 831 (1959)].
[22] J. W. McClure, Phys. Rev. 108, 612 (1957).
[23] Particularly lucid descriptions of this theory have been given by R. R. Haering and S. Mrozowski, *Progress in Semiconductors* (Heywood and Company, New York, 1960), Vol. 5, p. 273, and J. W. McClure, IBM J. Res. Develop. 8, 255 (1964).
[24] P. Nozières, Phys. Rev. 109, 1510 (1958).
[25] J. D. Bernal, Proc. Phys. Soc. (London) A106, 749 (1924).
[26] R. W. G. Wyckoff, *Crystal Structures* (Interscience Publishers, Inc., New York, 1960), Vol. I.

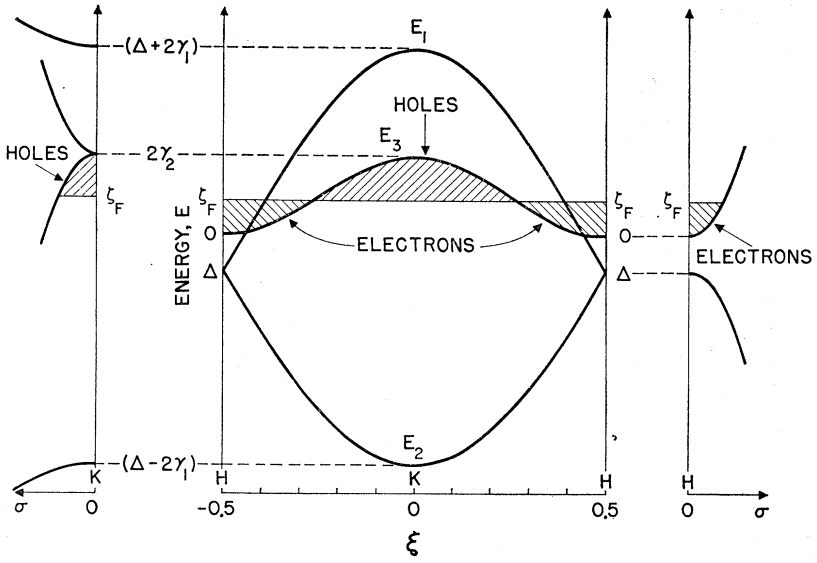

FIG. 3. Energy bands of graphite near the vertical zone edge HKH at zero field as given by the Slonczewski-Weiss model. The coordinates ξ along the k_z direction and σ in the k_z plane are the reduced wave vectors defined in the text. The E_3 band is doubly degenerate for $\sigma=0$. The majority hole pocket near $\xi=0$ is formed by the E_3 band for which $dE/d\sigma<0$, and the majority-electron pocket near $\xi\simeq 0.35$ is formed by the other E_3 band for which $dE/d\sigma>0$.

lattice, we shall use the dimensionless cylindrical coordinates (σ,α,ξ) with the origin at point K. Distances measured in the k_x and k_y directions in k space are given by $k_x=-(2\sigma/3^{1/2}a_0)\sin\alpha$ and $k_y=(2\sigma/3^{1/2}a_0)\cos\alpha$, while vertical distances are given by $k_z=2\pi\xi/c_0$.

In the absence of an applied magnetic field the effective-mass Hamiltonian for the four π bands can be written as[22]

$$\mathcal{H}=\begin{bmatrix} E_1 & 0 & H_{13} & H_{13}^* \\ 0 & E_2 & H_{23} & -H_{23}^* \\ H_{13}^* & H_{23}^* & E_3 & H_{33} \\ H_{13} & -H_{23} & H_{33}^* & E_3 \end{bmatrix} \tag{3}$$

in which

$$\begin{aligned} E_1&=\Delta+\gamma_1\Gamma+\tfrac{1}{2}\gamma_5\Gamma^2, \\ E_2&=\Delta-\gamma_1\Gamma+\tfrac{1}{2}\gamma_5\Gamma^2, \\ E_3&=\tfrac{1}{2}\gamma_2\Gamma^2, \\ H_{13}&=2^{-1/2}(-\gamma_0+\gamma_4\Gamma)\sigma\exp(i\alpha), \\ H_{23}&=2^{-1/2}(\gamma_0+\gamma_4\Gamma)\sigma\exp(i\alpha), \\ H_{33}&=\gamma_3\Gamma\sigma\exp(i\alpha), \end{aligned} \tag{4}$$

and $\Gamma=2\cos(\pi\xi)$.

In general, the energy bands have trigonal symmetry about the vertical edges of the Brillouin zone, but if γ_3 is neglected, they then have circular symmetry and can be described by

$$E=\tfrac{1}{2}(E_1+E_3)\pm[\tfrac{1}{4}(E_1-E_3)^2+\gamma_0^2(1-\nu)^2\sigma^2]^{1/2}, \tag{5a}$$

$$E=\tfrac{1}{2}(E_2+E_3)\pm[\tfrac{1}{4}(E_2-E_3)^2+\gamma_0^2(1+\nu)^2\sigma^2]^{1/2}, \tag{5b}$$

in which $\nu=\gamma_4\Gamma/\gamma_0$. This indicates that at the vertical zone edge where $\sigma=0$, the energy levels are given by the first three formulas of Eq. (4). A plot of these energy levels as a function of ξ is shown in Fig. 3 for the reduced zone scheme. The two E_3 bands are degenerate only along the edges HKH and the bounding planes $\xi=\pm 0.5$, whereas the E_1 and E_2 levels are degenerate only on the bounding planes $\xi=\pm 0.5$. Figure 3 indicates that a hole pocket is formed near $\xi=0$ by the E_3 bands for which $\partial E/\partial\sigma<0$; an electron pocket is formed along the zone edge, with an extremal area near $\xi=\pm 0.35$ by the other E_3 band for which $\partial E/\partial\sigma>0$. Electrons are also contained in a pocket formed by the E_1 band near $\xi\pm 0.5$. This pocket is shown in Fig. 2 as the "nose" of the "rocket-shaped" electron pocket in an extended zone scheme.

An expression for the extremal, cross-sectional area of the hole Fermi surface in the $k_z=0$ plane can be found from the Hamiltonian Eq. (3) and is given by

$$\begin{aligned} A_h&=4\pi\sigma_F^2/3a_0^2 \\ &=(4\pi(1+\nu)^2/3a_0^2\gamma_0^2)(2\gamma_2-\zeta)(\Delta+2\gamma_1+2\gamma_5-\zeta), \end{aligned} \tag{6}$$

if trigonal warping is neglected. The effective mass corresponding to this cross section is

$$m_h^*=\frac{\hbar^2}{2\pi}\frac{\partial A}{\partial\zeta}=-\frac{4\hbar^2(1+\nu)^2}{3a_0^2\gamma_0^2}(\tfrac{1}{2}\Delta+\gamma_1+\gamma_2+\gamma_5-\zeta). \tag{7}$$

The effects of trigonal warping on A_h and m_h^* are small[22,10] and are discussed in Sec. VI.

According to this picture, the Fermi surface therefore has three extremal cross sections for B along the c axis: $\xi=0$ corresponds to the maximal area of the hole pocket, and $\xi\approx\pm 0.35$ correspond to identical maximal areas of the two electron pockets. Another point of interest is at the hexagonal face of the Brillouin zone. As can be deduced from Eq. (5a), the Fermi surface of the electrons in the E_3 band coincides with the Fermi surface of the electrons in the E_1 band at $\xi=\pm 0.5$. Thus the nose of the rocket in Fig. 2 joins smoothly onto the rocket body. However, this area at zero field is *not* stationary at the Brillouin zone bound-

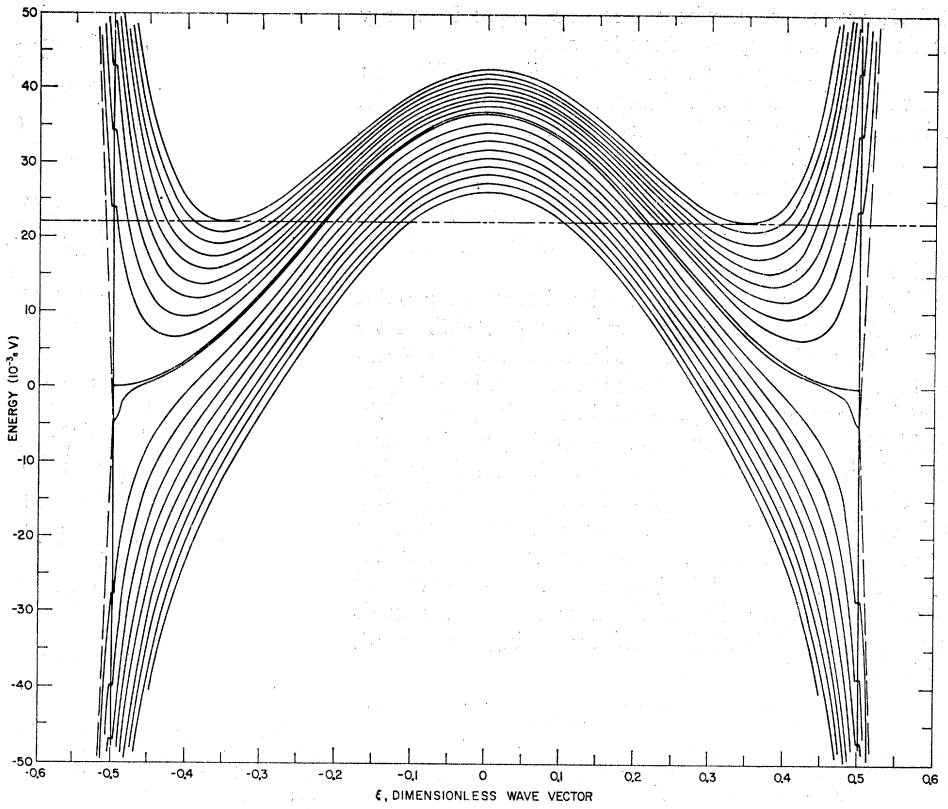

FIG. 4. Magnetic energy levels at the vertical zone edge given by the solution of the McClure-Inoue equation for $B=5$ kG and the band parameters of Table I. Only several of the levels with the lowest quantum numbers are shown. Dashed lines indicate the E_1 and E_2 energy bands at zero field (compare with Fig. 3) for an extended zone scheme. The sinusoidal curve at the center (with $E=0$ at $\xi=\pm 0.5$) is a field-independent energy level and corresponds to the E_3 band at zero field. The horizontal line represents the Fermi level, which occurs at $E=\zeta=0.022$ eV for PG.

ary; i.e., $\partial A/\partial\xi\neq 0$ at $\xi=\pm 0.5$, and therefore DHVA oscillations would not ordinarily be expected to arise from this location on the Fermi surface.

The effective-mass Hamiltonian in a magnetic field was derived by McClure[12] and Inoue,[13] and the matrix elements of this Hamiltonian are given by

$$\mathcal{H}=\begin{bmatrix} E_1 & 0 & H_{13}' & H_{14}' \\ 0 & E_2 & H_{23}' & H_{24}' \\ H_{13}' & H_{23}' & E_3 & 0 \\ H_{14}' & H_{24}' & 0 & E_3 \end{bmatrix}, \tag{8}$$

where

$$\begin{aligned} H_{13}' &= -(Q/2)^{1/2}(1-\nu)(n+1)^{1/2}, \\ H_{14}' &= -(Q/2)^{1/2}(1-\nu)n^{1/2}, \\ H_{23}' &= +(Q/2)^{1/2}(1+\nu)(n+1)^{1/2}, \\ H_{24}' &= -(Q/2)^{1/2}(1+\nu)n^{1/2}. \end{aligned} \tag{9}$$

Equation (9) employs the abbreviations $Q=3a_0^2\gamma_0^2(eB/2\hbar c)$ and $\nu=\gamma_4\Gamma/\gamma_0$. In order to obtain this Hamiltonian, the Luttinger-Kohn transcription[27] was used and the band interactions involving γ_3 were neglected. The secular equation associated with the Hamiltonian Eq. (8) can be written as[12,13]

$$(n+\tfrac{1}{2})Q=\frac{E-E_3}{2}\left[\frac{E-E_1}{(1-\nu)^2}+\frac{E-E_2}{(1+\nu)^2}\right] \pm\left\{\left[\frac{E-E_3}{2}\left(\frac{E-E_1}{(1-\nu)^2}-\frac{E-E_2}{(1+\nu)^2}\right)\right]^2+\frac{Q^2}{4}\right\}^{1/2}. \tag{10}$$

This McClure-Inoue equation has been solved with a digital computer to obtain the magnetic energy levels for an arbitrary value of ξ along the zone edge. The results for a field of $B=5$ kG are illustrated in Fig. 4. For a given quantum number n there are four magnetic energy levels, and these are shown for several of the lowest quantum numbers. The bands which correspond to E_1 and E_2 in Fig. 3 for $B=0$ are shown as dashed curves for $|\xi|>0.5$ in this extended zone scheme. The band which corresponds to E_3 for $B=0$ is the solid, sinusoidal curve for $|\xi|\leq 0.5$. Holes occupy the energy levels with negative curvature immediately below the E_3 curve near $\xi=0$, and electrons occupy the lower energy levels with positive curvature near $\xi\approx\pm 0.35$. As the magnetic field increases, these levels spread apart and eventually pass through the Fermi level at at energy $\zeta=0.022$ eV. DHVA oscillations due to the majority electrons and holes are associated with the extremal areas of the Fermi surface at $\xi=0$ and $\xi\approx$

[27] J. M. Luttinger and W. Kohn, Phys. Rev. **97**, 869 (1955).

± 0.35, respectively, where also the magnetic energy levels are stationary as a function of ξ.

McClure[12] has pointed out that if the term $\frac{1}{4}Q^2$ under the radical in Eq. (10) is ignored (the low-field limit), this secular equation for the magnetic energy levels becomes identical to the secular equation in the absence of the magnetic field except that $\gamma_0^2\sigma^2$ is replaced by $(n+\frac{1}{2})Q$. This is an example of the Onsager-Lifshitz condition for a DHVA oscillation given by Eq. (2) with the parameter $\gamma=\frac{1}{2}$.

Figure 4 shows that an additional stationary point of the magnetic energy levels exists at $\xi=\pm 0.5$. As we remarked earlier, the cross-sectional area of the Fermi surface in zero field is not extremal at this point, so that in the absence of spin-orbit interaction, no DHVA oscillation would be expected according to the usual prescription. However, as is shown in the Appendix, the singularity in the density of states associated with this stationary point of the energy levels is sufficient to give rise to DHVA oscillations, even in the absence of an extremal area.[28] At $\xi=\pm 0.5$ there is no trigonal warping (i.e., $\gamma_3\Gamma=0$) and the energies of these levels can be obtained from Eq. (10) by setting $\Gamma=0$, $v=0$, and $E_1=E_2$, with the result[12]

$$E=(\Delta/2)\pm[(\Delta/2)^2+(n,\, n+1)Q]^{1/2}. \qquad (11)$$

Although trigonal warping is neglected in Eqs. (6)–(8), the energy levels given by Eq. (11) are exact. There are four different energy levels associated with each quantum number n, and all but two are doubly degenerate. The condition $E=\zeta$ would define the values of B for which DHVA oscillations are expected; this condition can be written as

$$4\pi\zeta(\zeta-\Delta)/3a_0^2\gamma_0^2=2\pi(n,\, n+1)eB/\hbar c. \qquad (12)$$

From Eq. (5a) we can show that the left side of Eq. (12) is simply the cross-sectional area A_m of the Fermi surface in the k_z plane at $\xi=\pm 0.5$. Therefore, Eq. (12) is the Onsager-Lifshitz condition analogous to Eq. (2) with $\gamma=0$. The fact that γ is not the free-electron value is an indication of the unusual nature of the magnetic energy levels near the zone corner.

To calculate the expected phase of the DHVA oscillations for the extended zone Fermi surface we cannot simply use Eq. (1), because the stationary point at $\xi=\pm 0.5$ for an extended zone scheme does not correspond to either a maxima or minima in the magnetic energy levels, but behaves like an inflection point. In Eq. (1), the quantities $\pm\pi/4$ must be replaced by zero, the average of the two values.[29] Therefore, since $\gamma=0$, the total field-independent phase of the oscillatory thermodynamic potential is zero.

From Eq. (12) we can calculate the effective mass of these DHVA oscillations for B along the c axis, if we apply the traditional formula $m^*=\hbar^2(\partial A/2\pi\partial E)_\zeta$ to the nonextremal area at $\xi=0.5$. We have

$$m_m^*=\frac{\hbar^2}{2\pi}\frac{\partial A}{\partial\zeta}=\frac{2\hbar^2(2\zeta-\Delta)}{3\gamma_0^2a_0^2}. \qquad (13)$$

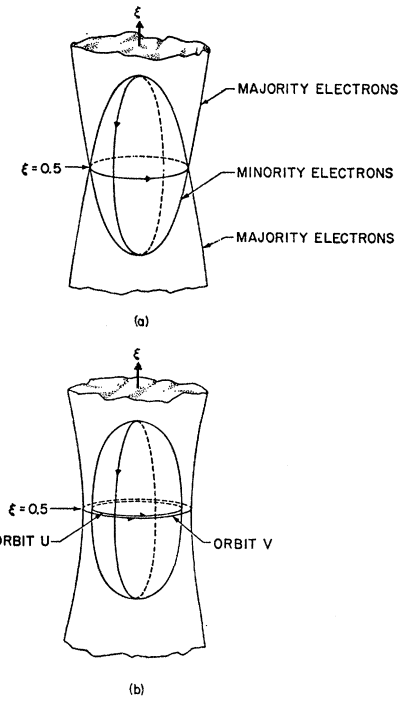

FIG. 5. Fermi surface near the Brillouin zone corner H in an extended zone scheme at zero field. (a) A minority carrier pocket is formed by the electrons which form the "noses" attached to the "rocket-shaped" pockets of the majority electrons. In the absence of spin-orbit coupling, the Fermi surface cross-sectional area in the k_z plane at $\xi=0.5$ is not stationary. (b) The presence of spin-orbit interactions separates the Fermi surface of the minority carrier pocket from the surface of the majority carriers, thus producing two nondegenerate extremal areas in the k_z plane at $\xi=0.5$.

So far we have considered only the extended zone description. Let us now consider the reduced zone picture. In effect, the Fermi surface near $\xi=0.5$ can be visualized by superimposing the surface in Fig. 2 with a similar surface obtained by a mirror reflection of the first through the hexagonal face at $\xi=0.5$. The interlocking rocket noses, defined by the electrons in the E_1 bands, form a Fermi surface such as that sketched in Fig. 5(a). The central pocket defined by the noses has a well-defined extremal area for all directions θ of the magnetic field relative to the k_z axis except for $\theta=0°$. However, since the calculations in the Appendix show that even for $\theta=0°$ DHVA oscillations are possible, the nose sections form a minority carrier pocket which should produce DHVA oscillations at all orientations of the field.

The extremal area for $\theta=90°$ can be calculated

[28] We wish to thank Dr. G. Dresselhaus for suggesting that this stationary point of the magnetic energy levels may give rise to DHVA oscillations.

[29] S. J. Williamson, Sc.D. thesis, Department of Physics, Massachusetts Institute of Technology, 1965 (unpublished).

simply from Eq. 5(a) provided that we assume that $c \ll 1$ and $c\gamma_2 \ll \gamma_1$, where $2c$ is the distance along the ξ axis between the tips of the minority carrier pocket. The result is

$$A_m(90°) = 16\zeta^{1/2}(\zeta-\Delta)^{3/2}/3^{3/2}\gamma_0\gamma_1 a_0 c_0. \quad (14)$$

From Eqs. (12) and (14) the DHVA period anisotropy is

$$\frac{P_m(0°)}{P_m(90°)} = \frac{A_m(90°)}{A_m(0°)} = \frac{4}{\pi 3^{1/2}}\left(\frac{a_0}{c_0}\right)\left(\frac{\gamma_0}{\gamma_1}\right)\left(\frac{\zeta-\Delta}{\zeta}\right)^{1/2}. \quad (15)$$

For simplicity, the minority carrier pocket can be approximated by an ellipsoid of revolution about the ξ axis with semi-axes a' in the ξ plane and c' along the ξ axis. The semi-axes are chosen so that the principal extremal areas at $\theta=0°$ and 90° are equal to the corresponding extremal areas of the pocket given by the Slonczewski-Weiss band model. Then the radii in the $\xi=0.5$ plane are identical for the two models (i.e., $a'=a$), but $c'=8c/3\pi$. A comparison of the two models is shown in Fig. 6. The dimensions along the ξ axis differ by about 15%.

The effect of spin-orbit interaction on the energy bands and on the Fermi surface near the Brillouin zone boundary $\xi=\pm 0.5$ has been calculated recently.[14] It is shown that both in zero field and in a magnetic field, all band degeneracies are lifted at the zone edge and at the Brillouin zone boundary $\xi=\pm 0.5$. In this plane, there are two unequal extremal cross sections, so that the nose of the rocket no longer fits smoothly on the body as indicated in Fig. 5(b). For $\theta=0°$, two DHVA periods are expected from electrons in the orbits U and V, corresponding to a maximal and a minimal cross-sectional area, respectively. For θ nonzero but small, two DHVA periods should be observed whether or not spin-orbit interactions are present.

IV. CHARACTERISTICS OF PYROLYTIC GRAPHITE SAMPLES

The PG samples used in the present experiments were grown and kindly furnished by Dr. R. J. Diefendorf of the General Electric Research Laboratories. They had been formed from carbon deposits obtained by cracking methane at 2250°C at low pressure.[30] The deposited material had been annealed at 3600°C for at least 4 h in an induction heater operating with a vapor pressure of 56 cm Hg. During annealing, the samples were pressed by kilogram weights. Only smooth pieces which showed no grain boundaries were used. The resulting PG samples had a typical dimension of 1 cm. Smaller pieces approximately 1 mm×3 mm×3 mm used in the experiments were cut from the large pieces with a sharp knife.

Measurements of the x-ray scattering angles from several (00l) reflections for Cu $K\alpha_1$ and Cu $K\alpha_2$ radiation yielded an interlayer spacing of 3.355±0.005 Å in PG[31] which is quite close to the spacing of 3.353 Å in SCG.[32] Back-reflection Laue patterns exhibited a series of concentric rings with no indications of appreciable alignment of the a axes of the crystallites.

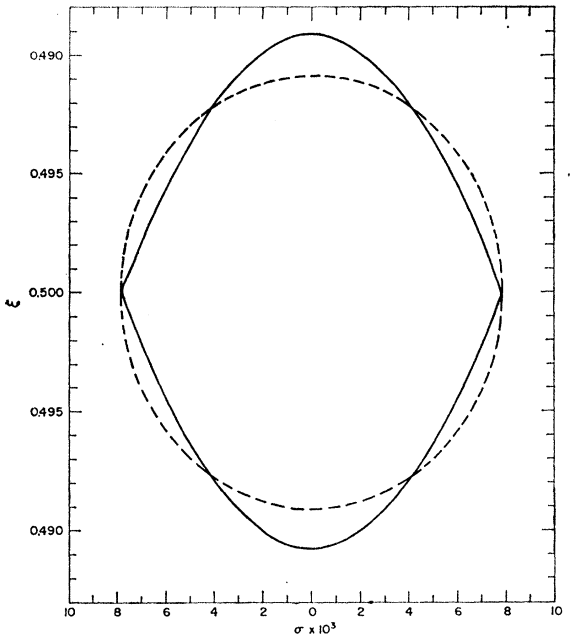

FIG. 6. Cross section in a ξ-σ plane of the Fermi surface of the minority-carrier pockets in PG. The dimensionless wave vectors ξ and σ are defined in the text. The solid line is predicted from the Slonczewski-Weiss model without spin-orbit coupling using the band parameters listed in Table I. The dashed line is for an ellipsoid having principal cross sectional areas equal to those of the Slonczewski-Weiss model.

The results of additional studies of the (002), (004), and (006) reflections in which the sample was rotated while keeping the scattering angle fixed are illustrated in Fig. 7. These samples were cut in the same manner and were of comparable size to the samples used in the DHVA experiments. The details of curves such as these varied for different samples, but the over-all widths of the diffraction peaks were reproducible to within 1.5°. In the absence of effects from a possible irregular surface, the intensity distribution of each curve would be interpreted as being approximately proportional to the orientation distribution $n(\delta)$ for the density of basal plane normals of the crystallites per unit solid angle. The angle δ is measured relative to the symmetry axis of the distribution; i.e., relative to the c axis of the sample. The half-width of the distribution at half-height is represented by the symbol δ_0. Of the traces shown in Fig. 7, the (002) trace should be more representative of the entire sample than the others because it was taken at a smaller scattering

[30] R. J. Diefendorf, J. Chimie Phys. 57, 815 (1960).

[31] We wish to thank Dr. O. J. Guentert of the Raytheon Company Research Laboratory for the initial x-ray analysis of our PG samples.

[32] A. W. Moore, A. R. Ubbelohde, and D. A. Young, Proc. Roy. Soc. (London) A280, 153 (1964).

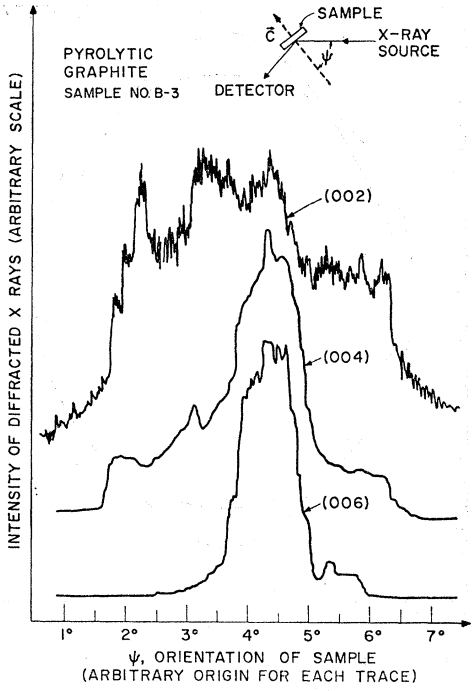

FIG. 7. X-ray studies of several (00l) reflections in pyrolytic graphite. The sample was rotated with the scattering angle fixed. Each trace was taken for a different scattering angle and initial sample orientation, but they are superimposed here for convenient comparison. The width of the distribution for each reflection is typical of the results obtained for several samples.

angle and hence more of the sample was exposed to the x-ray beam [the grazing angle is only about 13.7° to produce the (002) reflection]. For this trace an area with dimensions of about 1 mm×4 mm was exposed. The former dimension decreased with increasing scattering angle.

X-ray studies indicate the degree of alignment only at the surface of the sample because the penetration depth of the x rays is much less than the sample thickness. Although the sample which was used for the x-ray studies in Fig. 7 had a surface which visually appeared to have a mirror-like finish, it was not perfectly flat. The surface undulation or the detailed surface roughness may be sufficient to cause the substantially larger width of the (002) reflection compared with the (006) reflection. The latter has a width which is comparable to that observed in well-annealed PG by Guentert and Klein[33] and is in agreement with the x-ray studies of Moore, Ubbelohde, and Young.[32] Guentert and Klein[33] have found that the distribution $n(\delta)$ for samples of PG produced at various annealing temperatures could be characterized by a function $\cos^m\delta$, where m is an integer which is indicative of the crystallite alignment. As deposited (or turbostratic) PG has $\delta_0 \approx 23°$ for the half-width, corresponding to $m=8$. PG annealed at 3000°C has δ_0 ranging from 15° to 5°, corresponding to $m=20$ to 200, respectively. However, annealing under stress or at substantially higher temperatures may cause m to reach several thousand, corresponding to a crystallite alignment of better than 1°. This latter value is in agreement with the (006) reflection trace shown in Fig. 7. The samples that were stress-annealed at high temperatures are considerably more ordered than as-deposited PG, and we will deal only with the former in the present paper.

As the PG annealing and deposition temperatures are raised not only does crystallite alignment increase, but the local order or the size of the individual crystallite increases.[2,34] For deposition temperatures below about 1800°C turbostratic PG has an average crystallite size in the layer plane of $\bar{L}_a \approx 90$ Å and along the c axis of $\bar{L}_c \approx 25$ Å, but if the deposition temperature is increased to 2500°C, $\bar{L}_a = 325$ Å, and $\bar{L}_c = 250$ Å. Stress-annealing such samples at 3500°C or above produces large crystallites for which x-ray studies indicate $\bar{L}_a \gtrsim 300\,000$ Å.[32]

Recently, Hennig[35] has applied a gold evaporation technique in order to facilitate electron microscopy studies of dislocations, adsorbed impurities, and point defects in samples of PG annealed at various temperatures. He found that both SCG and PG have large concentrations of screw dislocations, with Burgers vectors parallel to the c axis. The magnitudes of the Burgers vectors (equal to the pitch) in SCG were never less than 450 Å, but in PG they were predominantly 3.55 Å; i.e., a monolayer step. The density of dislocations in PG is sensitive to the annealing temperature, being greater than 5×10^8 cm^{-2} in material annealed under pressure at 3100°C and about 10^6 cm^{-2} when annealed at 3600°C. The latter density corresponds to a mean spacing between dislocations of about 100 000 Å, which is about the in-plane size of the crystallites ($\bar{L}_a$) as determined by Moore, Ubbelhode, and Young.[32]

To extend investigation of the degree of crystallite alignment to the bulk sample we have performed neutron-diffraction studies on several samples of PG.[36] The penetration depth of the thermal neutrons was much greater than the sample dimensions, so that the intensity distribution was characteristic of the entire sample. As was done for the x-ray studies, the sample was rotated with a fixed scattering angle. A lead monochromator restricted the incident neutrons to a wavelength region centered at 1.20 Å with a spread of wavelengths of less than 0.5%. As indicated by diffraction experiments on a (111) reflection from a germanium single crystal, the collimation system and monochromator gave a resolution of 5 min for our experi-

[33] O. J. Guentert and C. A. Klein, Appl. Phys. Letters **2**, 125 (1963).

[34] O. J. Guentert, J. Chem. Phys. **37**, 884 (1962).

[35] G. R. Hennig, Science **147**, 733 (1965); Appl. Phys. Letters **4**, 52 (1964).

[36] We are indebted to Professor C. G. Shull for the use of his apparatus at the Massachusetts Institute of Technology Reactor and for his guidance of our neutron-diffraction investigations.

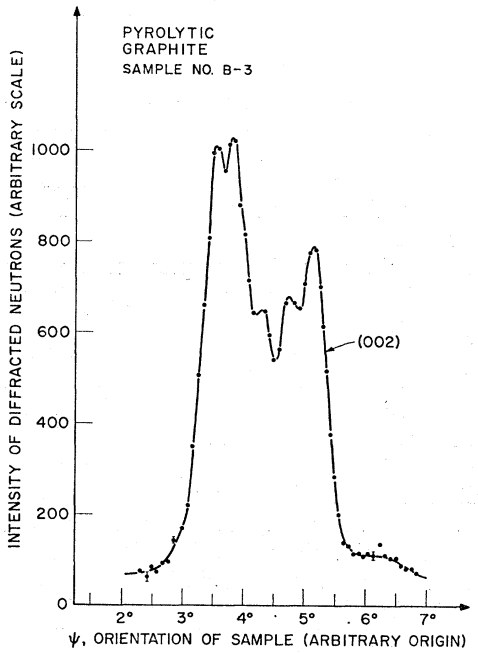

FIG. 8. Neutron diffraction study of the (002) reflection for the same sample of pyrolytic graphite as was characterized by the x-ray studies summarized in Fig. 7. The sample was rotated with the scattering angle fixed. Angular resolution is better than 5 min. All the samples investigated produced structure in the diffraction pattern.

ments on PG. The results shown in Fig. 8 were obtained for the (002) reflection from the same sample of PG as was used for the x-ray studies of Fig. 7. The ordinate represents the number of neutrons diffracted at an angle of about 20.5° for a fixed number of incident neutrons. The distribution shown in Fig. 8 is typical of our results from other samples of PG in that the distributions were not smooth, but exhibited structure. This may indicate that upon annealing at high temperature, crystallites tend to align quite well in local regions, but that the relative alignment of the local regions is not improved. Distributions from other samples had half-widths at half-height as large as $\delta_0 \approx 2°$.

If the x-ray data is indicative of crystallite alignment rather than surface roughness, comparison of the (002) reflections in Figs. 7 and 8 indicates that the crystallites in the bulk material are better aligned than those near the surface. Furthermore, comparison of the (004) and (006) x-ray reflections with the (002) neutron reflection indicates that small, local regions ($\sim$2 mm$\times$0.1 mm $\times$0.05 mm) are well aligned compared with the bulk sample.

We conclude that the actual distribution of crystallite c-axis orientations in the bulk sample is similar to the intensity distribution in Fig. 8, although the details of the structure and the width of the distribution will vary for different samples. The half-width of the distribution is $\delta_0 \approx 1°$, which is in agreement with previously published x-ray studies.[32,33] There was no detectable alignment of the a axes of the crystallites as indicated by x-ray Laue patterns.

V. EXPERIMENTAL DETAILS

All experiments were conducted in either 60- or 80-kG superconducting magnets using the low-frequency field-modulation technique.[37] A small ac modulating field was superimposed parallel to the larger dc applied field B, and the resulting time-dependent magnetization of the sample was monitored by synchronously detecting the voltage induced in a pickup coil surrounding the sample. A suitable arrangement of additional coils, a phase shifter and attenuator were used to buck out the voltage directly induced in the pickup coil by the modulation field. A modulation frequency of about 140 cps was used, and the induced voltage in the pickup coil was synchronously detected at the modulation frequency by a phase-sensitive detector. For small modulation amplitudes, the voltage induced in the pickup coils is proportional to the differential susceptibility dM/dB. Before recording, the rectified and filtered voltage from the detector was differentiated with respect to time, when necessary, to eliminate a slowly varying monotonic background signal.

Samples were mounted in a nonmetallic rotator[29] with Flexrock No. 80 cement. The rotator was then fitted inside the pickup coil, and the whole assembly was suspended in the tail section of a small glass Dewar which was inserted inside the superconducting magnet. Sample temperatures extending from 4.2 to 1.2°K could easily be achieved by pumping on the liquid helium in the glass Dewar.

The magnetic field was calibrated to an accuracy of better than 1% by the EPR of diphenylpicrylhydrazyl at 35 and 70 Gc/sec, and the field was linear with solenoid current to better than 1% for the fields utilized. The trapped flux in the solenoid was negligible at the location of the sample. Data was recorded on an X-Y recorder and on a two-channel strip chart recorder with the field signal being represented by the voltage developed across a current shunt in series with the magnet.

DHVA oscillations were observed in the differential magnetic susceptibility of both PG and SCG[38] for $\mathbf{B}$ along the c axis and in PG as a function of θ, the angle between $\mathbf{B}$ and the c axis. A typical recorder trace for $\theta = 0°$ is shown in Fig. 9. Long-period oscillations with a period $P \approx 2\times10^{-4}$ G^{-1}, associated with a pocket of minority carriers, were observed in the field range $300 \lesssim B < 2$ kG. At each orientation of the field relative to the sample, the period was determined from the number of oscillations occurring in a known field

[37] A. Goldstein, S. J. Williamson, and S. Foner, Rev. Sci. Instr. **36**, 1356 (1965).

[38] We are grateful to Dr. R. J. Diefendorf of the General Electric Research Laboratories for providing samples of PG and to Dr. D. E. Soule of the Union Carbide Research Laboratory for providing several samples of SCG.

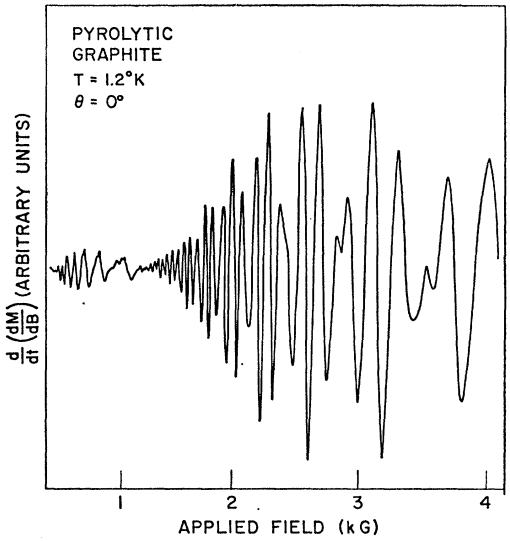

FIG. 9. Typical low-field experimental data from pyrolytic graphite for B along the c axis ($\theta=0°$). The quantity dM/dB is the differential susceptibility. One differentiation with respect to time (for an increasing field sweep) was taken before recording to eliminate a monotonic background. Minority carrier DHVA oscillations are exhibited at fields below about 1 kG and majority-electron and hole-DHVA oscillations appear at higher fields.

interval. At high fields a beat pattern was evident due to the superposition of two sets of oscillations having periods about 10 times shorter than the period of the minority carrier. These oscillations were attributed to the majority electrons and holes which are located near the extremal cross-sectional areas of the pockets shown in Fig. 2. For the trace shown in Fig. 9 the signal from the phase-sensitive detector was differentiated with respect to time before it was recorded. Owing to the B^{-1} periodicity, consecutive oscillations occur between larger increments of both field and time, and therefore at high fields the observed amplitude of a particular DHVA oscillation decreases for a given amplitude of the modulation field and for the linear sweep rate of the magnetic field. Similar traces were taken with PG for various angles θ, but since no oscillations were observed for $\theta>80°$, no attempt was made to determine the azimuthal dependence of the DHVA effect.

VI. MAJORITY CARRIERS

To obtain precise comparisons of the extremal areas of the Fermi surface in PG and SCG we have made direct comparisons of the DHVA effect observed in PG and in SCG for $\theta=0°$ in the field range 2 kG$\lesssim B\lesssim$20 kG and at a temperature of $T=1.2°$K. Repeated measurements on different samples of PG and SCG showed that the maxima, minima, and inflection points of the majority carrier DHVA oscillations occurred at the same fields for PG as for SCG to within a 2% experimental uncertainty. The beat patterns between the hole- and electron-DHVA oscillations were qualitatively similar indicating that the field-dependent amplitude of their individual oscillations are identical. For PG and SCG the amplitude of the DHVA oscillations, normalized to samples of equal weight, was about 20% lower in PG than in SCG. In Sec. VII we shall show how this 20% reduction can be explained by collisions at crystallite boundaries which simply limit the number of electrons contributing to the DHVA effect.

Figure 10 shows an integer plot for the magnetic field at which the differential susceptibility exhibits a sharp peak. Comparison of the sign of these sharp peaks in the *differential susceptibility* with a calibration signal from a ferromagnetic sample and with the observed *magnetization* of a PG sample using a vibrating sample magnetometer has established that these sharp peaks are *maxima* of dM/dB. Only the electron maxima were directly observed except possibly at $B\approx32$ kG, where a hole maxima may have been observed. It can easily be shown that sharp peak in dM/dB occurs whenever the thermodynamic potential in Eq. (1) has a sharp peak, so that in this sense Ω and the differential susceptibility have identical phase. The straight line drawn through these points yields a DHVA period of $(2.08\pm0.02)\times10^{-5}$ G^{-1} and intercepts the ordinate at $B^{-1}=0$ with a phase of $2\pi(0.38\pm0.05)$.

From the observed DHVA beat pattern, the period of the majority-hole oscillations was determined to be $(1.51\pm0.03)\times10^{-5}$ G^{-1}. A sequence of integers deduced from the location of the observed nodes and antinodes was fitted to a straight line which had the correct slope for the period. The resulting line intercepted the ordinate at $B^{-1}=0$ with a phase $2\pi(0.32+0.09)$, as is shown in Fig. 10.

From analysis of the DHVA oscillations in SCG for $\theta=0°$,[7] the period and effective mass, respectively, have been found to be $(2.07\pm0.04)\times10^{-5}$ G^{-1} and 0.039 m_0 for the electron and $(1.51\pm0.03)\times10^{-5}$ G^{-1} and 0.057 m_0 for the hole.

Since our previous discussion in Sec. II indicates that the hole- and electron magnetic energy levels pass through the Fermi surface at positions where the cross-sectional area is a maximum (at $\xi=0$ and $\xi\approx\pm0.35$, respectively) with $\gamma=\frac{1}{2}$ in Eq. (1), the predicted low-field phase for both the hole and electron oscillations is $2\pi(+\frac{3}{8})=2\pi(0.375)$. This excellent agreement with the experimental values shows that electron-electron interactions[39] do not seriously disturb the phase of the DHVA oscillations in graphite.

Deviations from strict B^{-1} periodicity in the high-field limit for the electron or hole maxima, could not be determined with sufficient precision to warrant detailed investigation. The spacing between maxima (about 20 kG) is so large in the low quantum limit that the differential susceptibility is too small for accurate measurements.

[39] J. M. Luttinger, Phys. Rev. **119**, 1153 (1960); **121**, 1251 (1961).

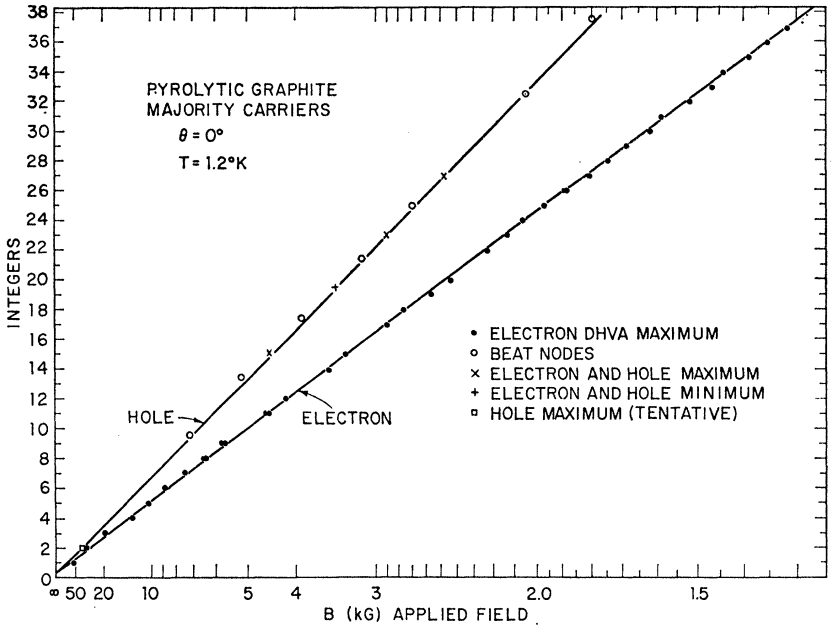

FIG. 10. Integer plot for the observed majority-carrier DHVA oscillations in pyrolytic graphite. The hyperbolic scale for the field results in a scale for the abcissa whose linear dimension with respect to the origin is proportional to B^{-1}. The periodicity in B^{-1} for the electron DHVA maxima is evident. The plot for the hole maxima and minima was deduced from the observed DHVA period and the locations of the amplitude nodes and antinodes, as is explained in the text.

A further comparison of the extremal areas of the Fermi surfaces of PG and SCG was made by studying the orientation dependence of the majority hole and electron periods, and the results are shown in Fig. 11. The solid curves represent the anisotropy of the majority hole and electron periods of SCG as determined by Soule, McClure, and Smith.[7] The dashed line for the hole period near $\theta=90°$ is an extrapolation from the SCG results.[7] The equality of the periods and therefore also of the extremal areas of the majority-electron Fermi surfaces in PG and SCG is seen for angles as large as $\theta=60°$. Similarly, the extremal areas of the Fermi surface of the majority hole in PG and SCG are identical for $\theta\lesssim 50°$. At larger angles the amplitude of the DHVA oscillations decreases markedly, and the beat pattern is less pronounced. Thus, no significant comparison between PG and SCG periods can be made for $\theta\gtrsim 70°$.

Several mechanisms are responsible for the reduction of the DHVA amplitudes as θ is increased. In SCG the effective mass of both the hole and the electron increases with increasing θ,[7] thus decreasing β^* in Eq. (1) and reducing the DHVA amplitude. Furthermore, in PG the amplitude is degraded by the increased carrier scattering due to interlayer imperfections, and by the destructive interference between DHVA contributions from misaligned crystallites, due to the anisotropic nature of the Fermi surface. These deleterious interference effects arise from both the c-axis orientation distribution $n(\delta)$ as will be discussed in the following section, and from the random alignment of crystallite a axes. The DHVA amplitude of the majority holes decreases relative to the amplitude of the electrons because the holes have a heavier effective mass and shorter period. At all angles, the dominant DHVA oscillation in PG is that from majority electrons.

From Eqs. (6) and (7) and expressions for the extremal area and effective mass of the majority-electron pocket, it is apparent that if the band parameters determining the majority-carrier periods in PG are identical to those in SCG, then the effective masses

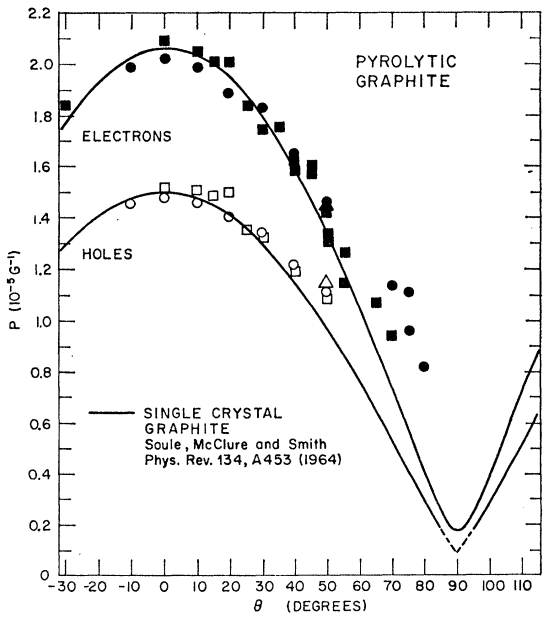

FIG. 11. Orientation dependence of the observed DHVA periods of the majority electrons and holes in pyrolytic graphite. The solid lines are the best-fit curves obtained by Soule, McClure, and Smith from Shubnikov–de Haas experiments on natural single-crystal graphite.

of these carriers are also equal. The qualitative similarity of the field dependence of the DHVA beat patterns in PG and SCG together with this deduction that the effective masses are respectively equal indicate that the respective Dingle temperatures are also comparable. This conclusion is further supported by the fact that for $\theta=0°$ the magnitude of the DHVA oscillations per gram of PG was only 20% less than the magnitude per gram of SCG. In the following section it is shown how this small difference can be explained by scattering of the carriers at crystallite boundaries. The Dingle temperature associated with carriers which are not subject to collisions with crystallite boundaries would then have values comparable to those obtained by the digital computer calculation of Soule, McClure, and Smith for SCG; namely, $T_D\approx0.7°$K for the elec- and $T_D\approx0.6°$K for the holes.

The equality of the extremal areas of the majority-hole and electron Fermi surfaces in PG and SCG can be exploited to evaluate certain band parameters of the Slonczewski-Weiss graphite band model. Starting with preliminary values of the band parameters for PG as determined by the magnetoreflection experiment[10] but neglecting γ_3, the DHVA periods for holes and electrons were calculated for $\theta=0°$ and $\theta=90°$. The band parameters were then adjusted to obtain agreement with the experimental values for the periods. The results of this calculation are summarized in Table I. Several of these parameters have previously been evaluated by McClure.[22] We have calculated the effect of trigonal warping on the $\theta=0°$ periods and effective masses to justify the approximation of $\gamma_3=0$, and the results are summarized in Table II for various values of γ_3 in the range $0\leq\gamma_3\leq0.30$ eV.

Calculation of the majority-hole period in SCG at $\theta=90°$ for various azimuthal angles φ of the field relative to the a axis indicates that for $\gamma_3=0.15$ eV, the period anisotropy is less than 5%. Trigonal warping is less pronounced for the majority electrons and may result in a period anisotropy of about 2%. Since the azimuthal dependence of the DHVA periods is seen to be small and, furthermore, since neither the electron nor hole periods at $\theta=90°$ were observed in PG, no attempt was made to study the φ dependence of the periods. No additional extrema of the cross-sectional area are introduced by the "fin" structures where the electron and hole surfaces touch (see Fig. 2). The effect of spin-orbit interaction on the "fin" structures is to round off the sharp corners.

To a first approximation, the period anisotropy in SCG and PG as a function of θ was characterized by the formula for ellipsoidal Fermi surfaces[7]:

$$P^2=C\cos^2\theta+D\sin^2\theta, \tag{16}$$

where C and D are experimentally determined constants. The electron curve for SCG[7] in Fig. 11 has a period anisotropy of 12.1:1, and the hole curve is for an ellipsoid of 12.1:1 anisotropy with an extrapolation for conical tips which increases the anisotropy to 17.3:1. The complicated "fin" structure of the electron rocket shown in Fig. 2, and associated with the band parameter γ_3 was not taken into account in the SCG analysis of Soule, McClure, and Smith. Since for SCG the second term in Eq. (16) is only 6% of the first at $\theta=70°$ due to the large anisotropy of the period, the large scatter in the PG data prohibited the determination of the quantity D with any significant reliability. Indeed, the PG data in Fig. 11 does not distinguish between a highly elongated ellipsoid and a cylindrical Fermi surface corresponding to a two-dimensional material.

The possibility that PG might actually have two-dimensional energy bands is of considerable interest. Recent Alfvén wave propagation experiments in graphite by Surma, Furdyna, and Praddaude[40] have dramatically pointed out the apparent two-dimensional nature

TABLE I. DHVA parameters for pyrolytic graphite. The calculated values are based on the Slonczewski-Weiss band model and the McClure-Inoue equation without spin-orbit interaction; the effects of trigonal warping have been neglected. The band parameters, expressed in units of electron volts, are as follows: $\gamma_0=3.13$, $\gamma_1=0.400$, $\gamma_2=0.0185$, $\gamma_3=0.0$, $\gamma_4=-0.250$, $\gamma_5=0.0185$, and $\Delta=-0.005$. The Fermi energy $\zeta=0.022$ eV was determined by the condition for carrier compensation $n_h=n_e+n_m$. P is the DHVA period, m^* is the effective mass, Φ is the field-independent phase of the oscillatory free energy, and n is the carrier concentration. The subscript e refers to the majority electron, h to the majority hole, and m to the minority electron.

	Observed	Calculated
$P_e(0°)$	$(2.08\pm0.02)\times10^{-5}$ G^{-1}	2.08×10^{-5} G^{-1}
$m_e^*(0°)$	$(0.039\pm0.001)m_0$[a]	$0.040\,m_0$
$\Phi_e(0°)$	$2\pi(0.38\pm0.05)$	$2\pi(0.375)$
$Pe(90°)$	$(0.15\pm0.03)\times10^{-5}$G^{-1}[a]	0.19×10^{-5}G^{-1}
n_e		3.34×10^{18} cm^{-3}
$P_h(0°)$	$(1.51\pm0.03)\times10^{-5}$ G^{-1}	1.51×10^{-5} G^{-1}
$m_h^*(0°)$	$(0.057\pm0.002)m_0$[a]	$0.053\,m_0$
$\Phi_h(0°)$	$2\pi(0.32\pm0.09)$	$2\pi(0.375)$
$P_h(90°)$		0.11×10^{-5} G^{-1}
n_h		n_e+n_m
$P_m(0°)$	$(2.24\pm0.03)\times10^{-4}$ G^{-1}	2.23×10^{-4} G^{-1}
$m_m^*(0°)$	$(4.0\pm0.4)\times10^{-3}\,m_0$	$4.24\times10^{-3}m_0$
$\Phi_m(0°)$	$2\pi(0.03\pm0.09)$	0
$P_m(90°)$	$(1.18_{-0.23}{}^{+0.02})\times10^{-4}$ G^{-1}	0.962×10^{-4} G^{-1}
n_m	$(7.5_{+1.8}{}^{-0.2})\times10^{15}$ cm^{-3}	9.1×10^{15} cm^{-3}

[a] Parameters obtained by Soule, McClure, and Smith from Shubnikov-de Haas experiments on single-crystal graphite.

TABLE II. Effect of γ_3 on DHVA parameters. The band parameters listed in Table I were used for these calculations and the Fermi energy ζ was taken to be independent of γ_3. Preliminary analysis of magnetoreflection data by Dresselhaus and Mavroides indicates that $\gamma_3\approx0.15$ eV.

γ_3 (eV)	P_e (10^{-5} G^{-1})	m_e^*/m_0	P_h (10^{-5} G^{-1})	m_h^*/m_0
0.00	2.08	0.0397	1.51	0.0527
0.10	2.08	0.0397	1.53	0.0529
0.15	2.07	0.0397	1.56	0.0533
0.20	2.07	0.0397	1.62	0.0544
0.25	2.06	0.0397	1.72	0.0567
0.30	2.06	0.0397	1.92	0.0627

[40] M. Surma, J. K. Furdyna, and H. C. Praddaude, Phys. Rev. Letters 13, 710 (1964).

of the mass-distribution function which is measured in their experiment on PG. Since their orientation experiments on PG indicated that only the component of the magnetic field perpendicular to the layer plane seems to influence the Alfvén wave interference pattern, they concluded that the absence of long-range order between layer planes effectively restricted out-of-plane carrier motion. We wish to emphasize, however, that the increased probability of scattering for the interplane carrier motion as compared with inplane motion need not imply that the Fermi surfaces of the carriers are cylindrical. In fact, if our interpretation for the origin of the minority-carrier oscillations discussed in Sec. VIII is correct, the electron Fermi surface in PG for an extended zone scheme is closed and is similar to that illustrated in Fig. 2. The applicability of the Slonczewski-Weiss band model to the DHVA effect in PG is verified by the good agreement obtained between the predicted and observed periods, period anisotropy, phase and effective masses for both the majority electron carriers. In addition, according to the Slonczewski-Weiss model, a closed electron surface implies a closed hole surface.

VII. LOCAL ORDER

The DHVA effect is usually not used to determine the degree of order in a material, because only nearly perfect crystals are studied in order to avoid deleterious effects. However, as was indicated in Sec. IV, PG is a polycrystalline material; the orientation distribution of crystallite c axes, $n(\delta)$, and the finite crystal size can have significant effects on the observed DHVA oscillations. In this section, we shall first use the DHVA effect to estimate the extent of local order or the crystallite size, and then we shall proceed to investigate one result of the orientation distribution of the crystallites. We shall regard PG as consisting of an assembly of crystallites, each with an identical band structure and with an average layer-plane dimension $\bar{L}_a$ and c-axis dimension $\bar{L}_c$.

If it is assumed that a carrier has little chance of crossing a crystallite boundary without scattering, the maximum diameter of the cyclotron orbit at fields for which the DHVA effect is observed can be used as a lower limit for the dimensions of each crystallite. The maximum orbit diameter for any orientation of **B** is determined from the minimum field at which DHVA oscillations are observed. Admittedly this will provide only a crude determination of the crystallite dimensions; the observed minimum field may, in fact, be determined by thermal damping [the $\sinh(2\pi^2kT/\beta^*B)$ factor in Eq. (1)] rather than by the collision time, but our procedure will still yield a valid lower limit for the crystallite dimensions. With $\theta=0°$, the majority-carrier oscillations were observed for fields as low as 1 kG, so that with $m^*\approx 0.04\,m_0$, and the average in-plane speed[2,41] of $v\approx 0.5\times 10^8$ cm/sec, the cyclotron diameter is 10 000 Å. This can be compared with the respective value for as-deposited PG which has $\bar{L}_a\approx 250$ Å.[2]

An estimate of the actual value of $\bar{L}_a$ can be deduced from the additional experimental fact that the DHVA amplitude per gram in PG was only 20% less than that observed in SCG for $\theta=0°$. If we assume that this reduction is exclusively due to collisions at crystallite boundaries, this means that 80% of the layer plane area of a PG crystallite must be farther than one cyclotron radius from the boundary of the crystallite. Consequently the crystallite diameter is about 10 times the cyclotron diameter, or $\bar{L}_a\approx 100\,000$ Å. This agrees favorably with the estimate of 300 000 Å for well-annealed PG obtained from x-ray data by Moore, Ubbelohde, and Young.[32]

Now we shall consider one of the effects of the orientation distribution of crystallite c axes. We shall assume that the distribution function $n(\delta)=\cos^m\delta$ adequately describes the orientation distribution of c axes and will neglect the structure shown in Fig. 8. Interference effects from the magnetizations from various crystallites might be expected to be most pronounced for large θ where the DHVA period varies rapidly with θ. Our attention will be focused on the region $70°\leq\theta\leq 80°$, where the DHVA amplitude decreases sharply and where the scatter in the experimental points increases substantially.

If we assume that the Fermi surface of the majority electrons in each crystallite is characterized by the DHVA period anisotropy of SCG (the upper curve in Fig. 11), then this period can be approximated by the linear relation

$$P=a\theta'+b \tag{17}$$

in the region of $40°>\theta>85°$. The angle θ' is the angle between **B** and a *particular* crystallite's c axis. Equation (17) agrees within 5% with the ellipsoid model of Eq. (16) if $a=-0.03\times 10^{-5}$ G^{-1} and $b=2.8\times 10^{-5}$ G^{-1}, where θ' is expressed in *angular degrees*.

If we retain only the leading term in the oscillatory potential of Eq. (1), the contribution to the magnetization M_i from a single crystallite with DHVA amplitude $M_0(B,\theta')$ can be expressed as

$$M_i=M_0(B,\theta')\sin\left[\frac{2\pi}{P(\theta')B}+\Phi\right], \tag{18}$$

where Φ is a constant. The total magnetization, M for all the crystallites in a sample of PG, which is characterized by the normalized distribution function $n(\delta)=G\cos^m\delta$, would then be

$$M=G\int_0^{\pi/2}d\delta\sin\delta\int_0^{2\pi}d\psi\cos^m\delta M_0(B,\theta')\times\sin\left[\frac{2\pi}{P(\theta')B}+\Phi\right], \tag{19}$$

[41] J. W. McClure, Phys. Rev. **112**, 715 (1958).

where ψ is the azimuth of a crystallite's c axis relative to the field **B**, measured in the plane perpendicular to the c axis of the sample, and where the normalization constant G is given by

$$G^{-1}=2\pi\int_0^{\pi/2} d\delta \sin\delta \cos^m\delta. \tag{20}$$

The relationship between θ, θ', δ, and ψ is given by

$$\cos\theta'=\cos\delta\cos\theta+\sin\delta\cos\psi\sin\theta, \tag{21}$$

where, as previously mentioned, θ is the angle between **B** and the average direction of the crystallites' c axes (the c axis of the sample). Since $m\approx 1500$ for our PG samples, the integrand in Eq. (19) is appreciable only for small values of δ, namely $\delta\lesssim 2°$; consequently, θ' and θ differ only a small amount ϵ defined by

$$\theta'=\theta+\epsilon. \tag{22}$$

Inserting this into Eq. (21) gives

$$\epsilon\approx-\sin\delta\cos\psi. \tag{23}$$

With the definition $P_0=(a\theta+b)$, with the neglect of the ϵ dependence of $M_0(B,\theta+\epsilon)$, and with $a\sin\delta/P_0\ll 1$, Eq. (19) becomes

$$M=M_0(B,\theta)\sin\left(\frac{2\pi}{P_0B}+\Phi\right)\times\left\{2\pi G\int_0^{\pi/2} d\delta\sin\delta\cos^m\delta J_0(x\sin\delta)\right\}, \tag{24}$$

where $J_0(\lambda)$ is the zeroth order Bessel function and $x=2\pi a/P_0^2B$. Interference effects are wholely described by the quantity in the brackets. In the limit $m\to\infty$ which corresponds to perfect crystallite alignment, it can be shown that this quantity approaches unity. Destructive interference (for finite m) occurs when $n(\delta)$ is appreciable for δ sufficiently large such that $J_0(x\sin\delta)$ assumes negative as well as positive values in the range of integration. The first zero $\lambda_1=2.4$ of $J_0(\lambda)$ defines the onset of destructive interference:

$$2\pi a\delta/P_0^2B\approx\lambda_1=2.4. \tag{25}$$

If we regard this as an upper bound on the half-width δ_0 of the distribution to avoid the onset of destructive interference, then for $\theta=70°$ and $B=10$ kG, we require

$$\delta_0<0.9°, \tag{26}$$

while for $\theta=80°$ and $B=20$ kG we require

$$\delta_0<0.6°. \tag{27}$$

These are stringent conditions. According to the neutron diffraction analysis discussed in Sec. IV, $\delta_0=1°$ and therefore Eqs. (26) and (27) are not satisfied by the present PG samples. The total magnetization for the majority electrons can be obtained explicitly from Eq. (24) by evaluating the integral:

$$M=M_0(B,\theta)\sin\left(\frac{2\pi}{P_0B}+\Phi\right)\left\{\pi G\left(\frac{x}{2}\right)^{-l}\Gamma(l)J_l(x)\right\}, \tag{28}$$

where $l=(m+1)/2$. From Eq. (28) we see that the effect of the crystallite orientation distribution $n(\delta)$ is to introduce a field-dependent factor in the amplitude of the DHVA oscillations, but leave the observed DHVA period unchanged. A more detailed analysis which includes the angular dependence of the amplitude would predict an increase in the DHVA period due to much larger DHVA amplitude at smaller values of θ.

According to the criterion in Eq. (25), the neutron-diffraction study indicates that a substantial degree of destructive interference reduces the observed DHVA amplitude in PG at large values of θ. In addition, the increased scattering due to interlayer motion and the orientation dependence of the effective mass[7] further reduce the amplitude.

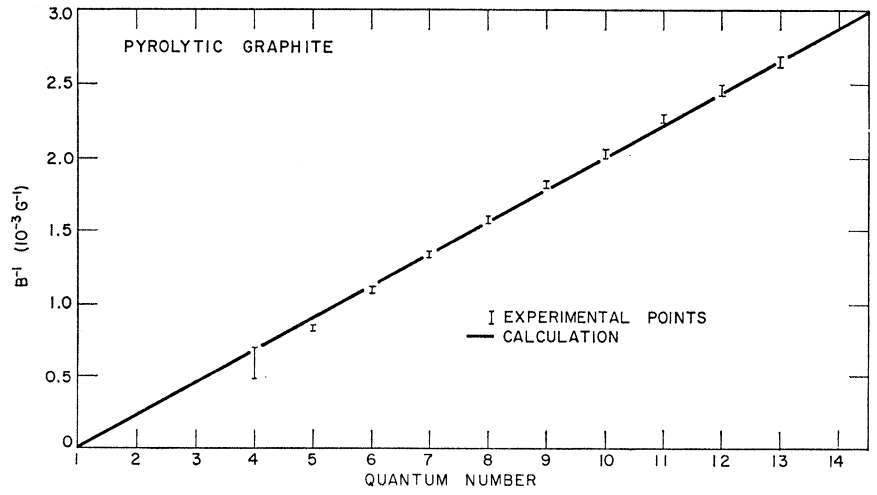

FIG. 12. Integer plot for the observed minority-carrier DHVA oscillations in pyrolytic graphite. The solid line is predicted from the Slonczewski-Weiss band model and the values of the band parameters listed in Table I.

VIII. MINORITY CARRIERS

One of the more important aspects of the present investigation is the observation and interpretation of a long-period oscillation due to minority carriers in PG. The present experiments also confirmed these oscillations first reported by Soule[8] for SCG, and the explanation for their origin has provided a sensitive verification for the Slonczewski-Weiss band model.

An integer plot for the DHVA oscillations observed in PG is shown in Fig. 12. The period of these DHVA oscillations is $(2.24\pm0.03)\times10^{-4}$ G^{-1}, which is an unusually long period and corresponds to a very small cross-sectional area. The phase at $B^{-1}=0$ is $2\pi(0.03\pm0.09)$.

Figure 13 illustrates the orientation dependence of the period observed in PG. A least-squares fit to an ellipsoidal model which is characterized by an orientation dependence of the form given in Eq. (16) is shown by the dashed curve. The period anisotropy defined by Eq. (15) is found to be $(1.9_{-0.1}{}^{+0.5}):1$, where the large upper uncertainty is imposed to cover the anisotropy of 2.4:1 obtained from a least-squares fit to only the data points for $\theta<45°$. It is believed that at large values of θ the strong dependence of the DHVA amplitude on θ together with the finite $n(\delta)$ orientation distribution of the crystallites might cause a slight bias of the observed DHVA periods toward higher values of the period. In addition, since the minority-carrier pocket of the Slonczewski-Weiss band model is not ellipsoidal as is explained in Sec. III, deviations by approximately 15% are expected from the orientation dependence of the period given by Eq. (16). For the Slonczewski-Weiss model, the period decreases more rapidly with increasing θ for small values of θ, than for the ellipsoidal model. The trend of the experimental points at small θ favors the Slonczewski-Weiss model.

The orientation dependence of the period for the minority-carrier oscillation observed by Soule[8] in SCG is indicated in Fig. 13, where we have normalized his period at $\theta=0°$ to coincide with our value for the period in PG. The period anisotropy of 9:1 determined by Soule is remarkably different from our value for PG. In addition, the magnitudes of the period at $\theta=0°$ for PG and SCG are quite different. We have confirmed Soule's results in SCG by conducting DHVA experiments at $T=1.2$°K and obtain an average value for the period of $P=(1.35\pm0.1)\times10^{-4}$ G^{-1}, which is in excellent agreement with Soule's result of $(1.35\pm0.3)\times10^{-4}$ G^{-1}.

The effective masses of the minority carrier in PG and SCG are also different. From the temperature dependence of the DHVA amplitude at $\theta=0°$, we obtain a value of $m^*=(4.0\pm0.4)\times10^{-3}m_0$ for PG; whereas, Soule has obtained a value of $m^*=2.3\times10^{-3}m_0$ for SCG. His value for m^* at $\theta=90°$ is $m^*=17\times10^{-3}m_0$ for SCG.

From the field dependence of the DHVA amplitude in PG at $\theta=0°$ and $T=1.2$°K, we have calculated the

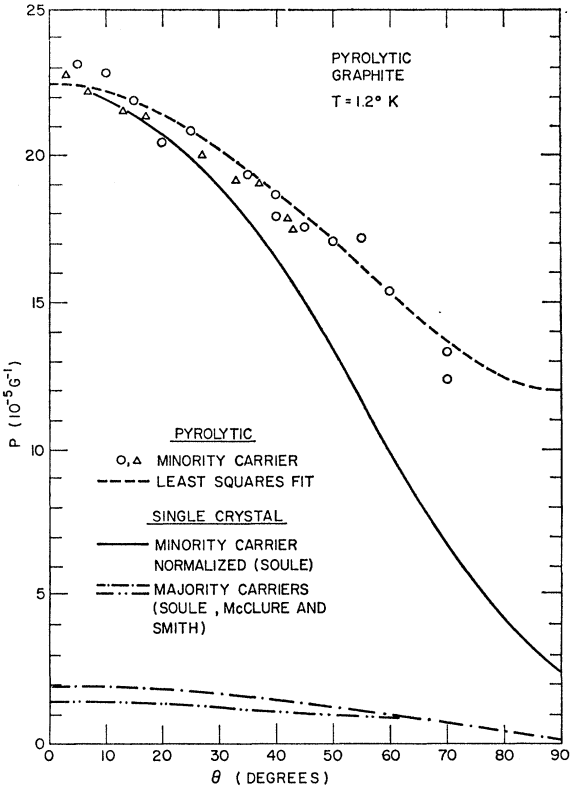

FIG. 13. Orientation dependence of the DHVA period of the minority carrier in pyrolytic graphite. The upper dashed curve is the least-squares fit assuming an ellipsoidal model for the Fermi surface. The solid curve is the best-fit curve obtained by Soule from DHVA experiments on natural single crystal graphite, which we have normalized to the period observed in pyrolytic graphite at $\theta=0°$. For comparison, the best-fit curves of Soule, McClure, and Smith for the periods of the majority carrier Shubnikov-de Haas oscillations are shown as the two lowest dashed curves.

Dingle temperature T_D in order to determine the linewidths of the quantum levels responsible for the minority-carrier oscillations. In addition to the factors in Eq. (1), we have included a factor to account for the response of the field-modulation technique.[29,37] The resulting value of $T_D=(1.5\pm0.1)$°K is about twice as high as the Dingle temperatures computed by Soule, McClure, and Smith[7] from the results of DHVA experiments on SCG majority carriers. The temperature of $T_D=1.5$°K corresponds to a Landau level linewidth of[17,18] $\pi kT_D\approx0.4\times10^{-3}$ eV, which is about 50 times smaller than the Fermi energy. If the linewidth is solely due to the lifetime of the quantum state, this lifetime is given by $\tau=\hbar/\pi kT_D\approx1.3\times10^{-12}$ sec.[17,18]

As stated in Sec. III, our interpretation for this minority-carrier DHVA oscillation involves the passage of magnetic energy levels through the Fermi level near the corner of the Brillouin zone. That this mechanism can produce DHVA oscillations for $\theta=0°$ is demonstrated in the Appendix. Using the band parameters listed in Table I, the field at which each oscillation

occurs has been calculated for $\theta=0°$ using Eq. (12); the straight line connecting these points in an integer plot is shown in Fig. 12. It can be seen that there is excellent agreement between the experimental data and the predictions of the Slonczewski-Weiss band model. It should be remarked that although the band parameters have been adjusted to optimize the agreement for both majority- and minority-carrier DHVA data, there are *no* adjustable parameters determining the phase.

The effective mass at $\xi=0.5$ for $\theta=0°$ in PG can be calculated from Eq. (13) and the band parameters in Table I. The result of $m_m^*=4.24\times10^{-3}m_0$ is in good agreement with the observed value of $m_m^*=(4.0\pm0.4)\times10^{-3}m_0$. The period anisotropy in PG has been calculated directly from the Slonczewski-Weiss model as 2.32, which is to be compared with the experimental value of $(1.9_{-0.1}^{+0.5})$. The result of 2.76 is obtained for the period anisotropy from the approximate formula Eq. (15). The close agreement between the observed DHVA period, phase, effective mass, and period anisotropy in PG supports our interpretation for the minority-carrier oscillation.

Our interpretation also predicts the existence of an additional DHVA oscillation over a limited angular range as B is tipped away from the c axis due to electrons orbiting on the body of the rocket near $\xi=\pm0.5$. At $\theta=0°$ this trajectory would coincide with the orbit around the pocket formed by the rocket noses. This has not yet definitely been observed in our experiments on PG, but Soule[8] has recently observed a second minority-carrier period for SCG over a range of θ.

An attempt was also made to calculate the DHVA periods, period anisotropies, and effective masses for SCG from the Slonczewski-Weiss band model, but no set of band parameters could be found which would be in agreement with the experimental values for SCG. On the other hand, for the PG data, several solutions of the Slonczewski-Weiss effective-mass Hamiltonian could, in fact, be obtained, which are consistent with the DHVA data. The particular solution given in Table I also satisfies the magnetoreflection data,[10] which measures a number of the band parameters more precisely and more directly. Since the periods of the majority carriers in SCG and PG are experimentally found to be identical within experimental error, those band parameters, which are determined by the majority periods were left unchanged to a first approximation. Thus, the large difference between the DHVA periods, effective masses, and period anisotropies for the minority-carrier oscillations in SCG and PG are, to a first approximation, attributed to large differences in Δ, the band parameter which most sensitively determines the properties of the Fermi surface near the hexagonal faces $\xi=\pm0.5$ of the Brillouin zone.

The band parameter Δ measures the difference in potential energy at the inequivalent A and B lattice sites in graphite, and can be related to overlap integrals two layer planes away. One would thus expect that $\Delta/\gamma_1\approx\gamma_1/\gamma_0$, since γ_0 and γ_1, respectively, depend on overlaps in the layer plane and one layer plane apart, from a tight-binding point of view. From such considerations one might expect $\Delta\approx0.05$ eV. However, Table I indicates that Δ for PG is one order of magnitude smaller than this estimate, indicating that energetically there is little distinction between A and B lattice sites, or that PG behaves like a two-dimensional solid in many respects. On the other hand, a preliminary band parameter determination based on the minority carrier period at $\theta=0°$ for SCG indicates that the order of magnitude of Δ for SCG agrees with the simple estimate made above. The results of such a fit are summarized in Table III.

To obtain more quantitative agreement in the period anisotropy for the long-period oscillations in SCG, it would seem that spin-orbit interaction could be invoked. In Fig. 5(b) it is seen that the effect of spin-orbit interaction is to separate the Fermi surface of the minority carriers from the Fermi surface of the majority carriers, so that for $\theta=0°$ two extremal cross-sectional areas are produced. Thus, the period anisotropy for the minority carrier is increased. Using the tight-binding arguments of McClure and Yafet[42] and the notation of Dresselhaus and Dresselhaus[14] for the three spin-orbit band parameters, the two larger parameters are taken to be equal while the third smaller one is neglected: i.e., $\lambda\equiv\lambda_{1,2^z}=\lambda_{3,3^z}$ and $|\lambda_{1,3}|\equiv0$. With these approximations, the relative change in the cross-sectional area associated with spin-orbit interaction $\delta A_m(0°)/A_m(0°)$ is given by[14]

$$\delta A_m(0°)/A_m(0°)=\pm\lambda\Delta/\zeta(\zeta-\Delta). \qquad (29)$$

From the temperature dependence of the g shift,[43] McClure and Yafet[42] have estimated $\lambda=2.2\times10^{-4}$ eV.

TABLE III. DHVA parameters for single-crystal graphite. The calculated values are based on the Slonczewski-Weiss band model and the McClure-Inoue equation without spin-orbit interaction; the effects of trigonal warping have been neglected. The band parameters, expressed in units of electron volts are as follows: $\gamma_0=3.13$, $\gamma_1=0.400$, $\gamma_2=0.0183$, $\gamma_3=0.0$, $\gamma_4=-0.250$, $\gamma_5=0.0183$, and $\Delta=-0.025$. The Fermi energy $\zeta=0.0214$ eV was determined by the condition for carrier compensation $n_h=n_e+n_m$. Calculated values for the majority-carrier parameters are all within 2% of those listed for PG in Table I, so only the minority-carrier parameters are given here. The notation is identical to that employed in Table I.

	Observed	Calculated
$P_m(0°)$	$(1.35\pm0.1)\times10^{-4}$ G^{-1}	1.35×10^{-4} G^{-1}
$m_m^*(0°)$	$2.3\times10^{-3}m_0$[a]	$5.8\times10^{-3}m_0$
$\Phi_m(0°)$		0
$P_m(90°)$	0.15×10^{-4} G^{-1} [a]	0.44×10^{-4} G^{-1}
n_m	$62\times10^{+15}$ cm^{-3} [a]	$31\times10^{+15}$ cm^{-3}

[a] Parameters obtained by Soule from DHVA experiments on SCG.

[42] J. W. McClure and Y. Yafet, *Proceedings of the Fifth Conference on Carbon* (Pergamon Press, Inc., Oxford and New York, 1962), p. 22.

[43] G. Wagoner, Phys. Rev. **118**, 647 (1960).

Thus, for SCG the change in the minority period at $\theta=0°$ is $\sim 1\%$, while the period for 90° is unaffected. In contrast, the relative change for PG is $\delta A_m(0°)/A_m(0°)\sim 4\times 10^{-3}$. Thus, this small value of λ cannot account for the large period anisotropy observed in SCG. On the other hand, if the period anisotropy is used to determine λ and Δ, then, for SCG, $\lambda\sim 0.016$ eV and $\Delta\sim 0.11$ eV. These values of λ and Δ are not satisfactory, partly because the discrepancy in $m_m^*(0°)$ indicated in Table III would be further increased. Therefore, the details of the minority-carrier Fermi surface in SCG are not yet understood. Further experimental investigations of the band structure near the zone corner are necessary to indicate whether the approximations leading to Eq. (29) are justified. A more quantitative study of the second long-period oscillation observed by Soule[8] should provide useful information about the relative change in $A_m(0°)$ and, therefore, its relation to the period anisotropy.

Soule[8] has shown that the minority-carrier period in SCG at $\theta=0°$ decreases by a factor of 2 with the addition of only 13 ppm of the acceptor boron. If each boron atom accepts one conduction electron, the density of holes introduced by the doping would be comparable to the density of holes in the intrinsic material ($\sim 1.5\times 10^{+18}$ cm^{-3}). However, despite this substantial doping, the majority-hole period seems to decrease by only about 20% and the majority-electron period seems to be essentially unaffected, indicating that the Fermi energy is relatively unchanged. These results are not quantitatively consistent with the predictions of a simple rigid-band model; consequently, it is not yet clear what the doping experiments imply.

McClure[44] has recently suggested that the minority-carrier oscillations may be due to small regions of rhombohedral graphite in the PG and SCG samples. Rhombohedral graphite differs from the more common hexagonal graphite in the stacking arrangement of the layer planes. Instead of the Bernal stacking sequency 1212$\cdots$ of the hexagonal form, the sequence 123123$\cdots$ is associated with the rhombohedral form. Regions of the latter sequence can be induced in the hexagonal structure by the application of the proper mechanical stress[45] and are occasionally found in the naturally occurring SCG. The band structure of the rhombohedral form has been investigated by Haering[46] and recently the theory has been extended by McClure[47] to include next-nearest layer interactions. Laves and Baskin[45] found that the rhombohedral form is metastable and can be eliminated from SCG by annealing at sufficiently high temperatures. Two hours annealing at 1500°C sufficed to eliminate artifically induced rhombohedral regions and 3000°C sufficed for naturally occurring regions. To investigate McClure's suggestion, two PG samples were re-annealed for three hours at 2800°C by Dr. Pappis at the Raytheon Company Research Laboratory in an attempt to eliminate possible rhombohedral regions. These samples were then carefully mounted in our apparatus and the DHVA experiments were repeated. Majority- and minority-carrier oscillations were observed with periods and amplitudes which were identical to those observed before re-annealing. This fact and the similarity of minority-carrier oscillations in different samples of PG indicate it is highly unlikely that the minority-carrier oscillations are due to regions of rhombohedral graphite.

[44] J. W. McClure (private communication).
[45] F. Laves and Y. Baskin, Z. Krist. **107**, 337 (1956).
[46] R. R. Haering, Can. J. Phys. **36**, 352 (1958).
[47] J. W. McClure (to be published).

IX. CONCLUSIONS

The present DHVA experiments have provided a detailed comparison of several aspects of the electronic band structure in SCG and well-annealed PG. The extremal cross-sectional areas of the electron- and hole-majority pockets in PG are, respectively, identical to within experimental error with those in SCG for θ as large as about 50°. When interpreted in terms of the Slonczewski-Weiss band model, this equality indicates that the band parameters γ_2, γ_1/γ_0^2, and γ_4 are the same for PG as for SCG. Minority-carrier DHVA oscillations observed in PG for $\theta=0°$ have been interpreted as arising from magnetic energy levels passing through the Fermi level at the hexagonal face $\xi=\pm 0.5$ of the Brillouin zone. Despite the fact that in zero field and in the absence of spin-orbit coupling this location does not correspond to an extremal area of the Fermi surface, a direct calculation of the free energy has shown that DHVA oscillations can be expected from a stationary point of the magnetic energy levels at $\xi=\pm 0.5$. From this interpretation and the DHVA data, band parameters of the Slonczewski-Weiss model for PG have been evaluated to yield results consistent with the preliminary analysis of magnetoreflection experiments by Dresselhaus and Mavroides. The close agreement between the predicted and observed DHVA period, effective mass, phase, and period anisotropy of the minority carrier has provided a sensitive verification of the applicability of the Slonczewski-Weiss model to PG. This agreement indicates that the hole and electron Fermi surfaces in PG are closed, and that the electron surface intersects the hexagonal face of the Brillouin zone. Differences in the DHVA data for the minority carriers in PG and those obtained by Soule for SCG indicate that although the general features of the majority-carrier pockets in these materials are comparable, the details of the Fermi surface near the zone corners are different. Assuming carrier compensation, band parameters could not consistently be fitted to both the DHVA data from SCG and the preliminary magnetoreflection analysis from PG even when the effects of spin-orbit interaction were included. The spin-orbit parameter so determined is about two orders of magnitude larger than that calculated by McClure

and Yafet from the g shift in EPR experiments, and the band parameter Δ for SCG would then have to be 20 times larger than that for PG.

The DHVA effect and neutron and x-ray diffraction have been used to study the degree of order of the crystallites in PG. The diffraction experiments indicate that the c axis of the crystallites are aligned to no better than $\sim 1°$. This misalignment indicates that the amplitude of the majority carrier DHVA oscillations in PG decreases markedly at large θ due to destructive interference between the magnetizations of variously oriented crystallites, as well as due to the anisotropy of the effective mass and the smaller mean free path for interlayer motion.

The analysis of DHVA experiments is conventionally based on Fermi surface models constructed from a nearly free electron approximation. For graphite, however, the Fermi surface has been successfully calculated from energy bands obtained from the symmetry properties of the hexagonal lattice. We have shown how specific band parameters can be determined consistent with the periods, effective masses and period anisotropies of all the observed DHVA oscillations in PG. In particular, the band structure model is even capable of accounting for the nonfree electron value of the phase of the minority-carrier DHVA oscillations. It is anticipated that similar band calculations for other materials may reveal aspects of the Fermi surface that heretofore have not been appreciated.

ACKNOWLEDGMENTS

One of the authors (S. J. W.) wishes to express his appreciation of Professor R. A. Smith for his constant encouragement and advice during the course of his thesis. We are indebted to Dr. G. Dresselhaus for his collaboration and illuminating comments and to Professor J. W. McClure, and Dr. J. G. Mavroides for many informative discussions and communications. We particularly wish to thank Dr. R. J. Diefendorf for providing the PG samples and Dr. D. E. Soule for providing the SCG samples. Appreciation is also due to Dr. J. Pappis for reannealing two PG samples, Dr. O. Guentert for carrying out the initial x-ray studies of one of our PG samples and for several educational discussions, and Professor C. G. Shull for guiding our neutron-diffraction investigations. We wish to thank Mrs. R. Sheshinski for some of the computer programming, E. Ferri for advice with x-ray studies, and D. Mullins for technical assistance.

APPENDIX A: OSCILLATORY-MAGNETIC-FIELD DEPENDENCE OF THE FREE ENERGY

In the absence of spin-orbit interactions, the cross-sectional area of the Fermi surface at the zone boundary, $\xi=0.5$, is not extremal according to the Slonczewski-Weiss band model. Nevertheless, this degenerate cross section gives rise to DHVA oscillations, as is shown here by direct computation. An oscillatory magnetic field dependence is found for the free-energy (and hence also for the magnetic susceptibility).[48] In particular, each oscillation can be identified with the passage of a magnetic energy level through the Fermi level at $\xi=0.5$.

The interest in this calculation is to establish that the criterion for the observation of a DHVA effect is not the existence of an extremal cross-sectional area of the Fermi surface, but rather a stationary point in the wave vector dependence of the magnetic energy levels. When spin-orbit interaction is included in the calculation of the topology of the Fermi surface, two extremal areas are found at $\xi=0.5$,[14] and the conventional DHVA theory[15] then applies to both of these cross sections:

The free energy per unit volume is given by[49]

$$F=\sum_i N_i\zeta-\frac{4eBkT}{\pi\hbar cc_0}\sum_{i=1}^{4}\int_0^{0.5}d\xi \times\sum_{n=0}^{\infty}\ln[1+\exp\{[\zeta-E_{i,n}(\xi)]/kT\}], \quad \text{(A1)}$$

in which ζ is the Fermi energy, $E_{i,n}(\xi)$ is the energy of the nth Landau level of the ith band at reduced wave vector $\xi=k_zc_0/2\pi$, and N_i is the carrier density of the ith band. The magnetic moment per unit volume is

$$M=-(\partial/\partial B)(F-\textstyle\sum_i N_i\zeta). \quad \text{(A2)}$$

The differential magnetic susceptibility is then defined as

$$\chi=(\partial M/\partial B)_\zeta; \quad \text{(A3)}$$

consequently, an oscillatory field dependence in F will produce an oscillatory field dependence in χ.

Since this calculation is designed to establish the existence of a DHVA effect associated with the passage through the Fermi level of the stationary point in the magnetic energy levels at $\xi=0.5$, we restrict the calculation to $T=0°$K. Furthermore, since magnetic fields of less than 2 kG are involved, the magnetic field dependence of ζ as well as DHVA contributions of majority electrons and holes can be neglected.

With these assumptions, the contribution to the free energy by the energy band E_1, which forms the minority electron pocket is

$$F_1=\frac{-4eB}{\pi\hbar cc_0}\sum_{n=0}^{n_{1F}}\int_{E_{1,n}(0.5)}^{\zeta}E(\partial E_{1,n}(\xi)/\partial\xi)^{-1}dE, \quad \text{(A4)}$$

[48] This calculation was carried out in collaboration with G. Dresselhaus and was reported by M. S. Dresselhaus, S. J. Williamson, and G. Dresselhaus, Bull. Am. Phys. Soc. **10**, 110 (1965).

[49] A. H. Wilson, *The Theory of Metals* (Cambridge University Press, London, 1953), 2nd edition, p. 160 ff.

in which n_{1F} is the quantum number labeling the highest magnetic energy level in band 1 which lies below the Fermi level for any value of ξ, and $E_{1,n}(0.5)$ is the value of the nth magnetic level of band 1 at $\xi=0.5$. The Fermi level energy is determined by requiring the number of electrons and holes to be equal. In order to calculate the integral in Eq. (A4), the derivative $\partial E_{1,n}(\xi)/\partial\xi$ is evaluated as a function of the variable of integration E. This is obtained by taking the derivative of the McClure-Inoue equation [Eq. (10)] with respect to ξ and solving for $\partial E_{1,n}(\xi)/\partial\xi$. Then by using an iterative procedure on the McClure-Inoue equation itself, the derivative $\partial E_{1,n}(\xi)/\partial\xi$ can be evaluated as a function of energy E. A rapidly converging procedure of numerical integration was used to compute the integral in Eq. (A4), except in the small energy range about the stationary point, where the integrand becomes singular. In this region between a cutoff energy $E_{1,n}(\xi_c)$ and the energy minimum $E_{1,n}(0.5)$ the integration was carried out explicitly by using a Taylor expansion about the singularity, thus obtaining

$$\int_{E_{1,n}(0.5)}^{E_{1,n}(\xi_c)} E(\partial E_{1,n}(\xi)/\partial\xi)^{-1}dE = -\tfrac{2}{3}[2E_{1,n}(0.5)+E_{1,n}(\xi_c)] \times\left[\frac{E_{1,n}(\xi_c)-E_{1,n}(0.5)}{2|\partial^2 E_{1,n}(\xi)/\partial\xi^2|_{\xi=0.5}}\right]^{1/2}. \quad \text{(A5)}$$

The term $|\partial^2 E_{1,n}(\xi)/\partial\xi^2|_{\xi=0.5}$ is found by solving for the second derivative of the McClure-Inoue equation at the stationary point $\xi=0.5$. The evaluation of the integral in Eq. (A4) does not depend on the choice of the energy cutoff $E_{1,n}(\xi_c)$.

Magnetic energy levels associated with one of the E_3 bands also have a stationary point at $\xi=0.5$ and pass through the Fermi level as the magnetic field is increased. The contribution to the free energy of these states is calculated in an analogous manner, although the details are somewhat different. A numerical calculation of the free energy was carried out in this way for the magnetic field range 700 G$<B<$1060 G and an oscillatory magnetic field dependence was found, which is illustrated in Fig. 14.

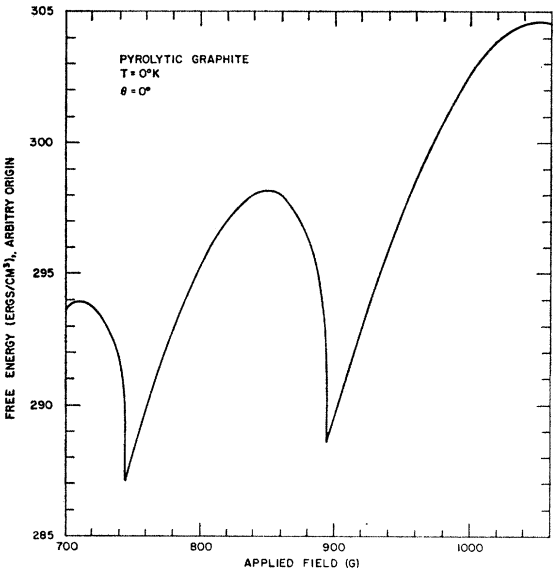

FIG. 14. Oscillatory free energy per unit volume at $T=0$°K associated with magnetic energy levels passing through the Fermi surface at $\xi=0.5$ when the applied field is parallel to the c axis. The calculations were based on first principles using the Slonczewski-Weiss band model and the magnetic energy levels of the McClure-Inoue equation. The locations of the sharp dips correspond to magnetic field values used to compute the straight line in Fig. 12. As defined in the text, these are identified with the observed sharp maxima in the differential susceptibility.

The contribution to the free energy of the stationary points in the magnetic energy levels at $\xi=0$ for the majority holes and at $\xi\approx0.35$ for the majority electrons can be calculated in exactly the same manner. Thus, by direct computation, the identification of the DHVA oscillations with stationary points in the magnetic energy levels is established. The existence of these DHVA oscillations has been established by consideration of the magnetic field dependence of the free energy. Since at low fields (i.e., $B\lesssim1$ kG) the Fermi energy is essentially independent of magnetic field, the more appropriate potential is the thermodynamic potential $\Omega=F-N\zeta$, which, in fact, exhibits sharp maxima as a magnetic energy level crosses the Fermi level.